

New Discotic Mesogens Based on Triphenylene-Fused Triazatruxenes: Synthesis, Physical Properties, and Self-Assembly

Baomin Zhao,[†] Bo Liu,[‡] Rui Qi Png,[‡] Kai Zhang,[†] Kheng Aik Lim,[†] Jing Luo,[†]
Jinjun Shao,[†] Peter K. H. Ho,[‡] Chunyan Chi,^{*,†} and Jishan Wu^{*,†}

[†]Department of Chemistry, National University of Singapore, 3 Science Drive 3, Singapore 117543
and [‡]Department of Physics, National University of Singapore, 2 Science Drive 3, Singapore 117542

Received September 28, 2009

A new type of discotic mesogen based on triphenylene-fused triazatruxenes was prepared by microwave-assisted 6-fold Suzuki coupling reactions from hexabromotriazatruxene, followed by FeCl₃-mediated oxidative cyclodehydrogenation. These disklike molecules showed extended π -conjugation, compared with the triphenylene and triazatruxene themselves. More importantly, they possess desirable HOMO energy levels, which allow efficient charge injection from electrodes such as gold electrodes. Their thermal behavior and self-assembly were studied by different techniques such as thermogravimetric analysis, differential scanning calorimetry, polarizing optical microscopy, and variable-temperature X-ray diffraction. These new discotic mesogens have very good thermal stability and show thermotropic liquid crystalline behavior. Ordered columnar liquid crystalline phase and crystalline phase were observed in both compounds with tunable phase transition temperatures and mesophase widths. The charge carrier mobilities of these extended triazatruxene samples were determined using the space-charge limited-current (SCLC) technique and high hole mobilities of 0.03 and 0.8 cm² V⁻¹ s⁻¹ were obtained for TP-TATC6 and TP-TATC12, respectively. Interestingly, the long-aliphatic-chain-substituted TP-TATC12 can gelate several nonpolar hydrocarbon solvents or polar aliphatic alcohol and ester solvents, because of strong intermolecular interactions. All these properties qualify this new type of discotic liquid crystals as potential hole transporting materials for electronic devices such as field-effect transistors, light-emitting diodes, and solar cells.

Introduction

The spontaneous self-assembly of molecules to form soft materials is currently a topic of great interest in areas that range from chemistry and biology to materials science.¹ Of the various soft materials, discotic liquid crystals (DLCs), first discovered by Chandrasekhar in 1977,² have attracted special attention, because the high one-dimensional (1D) charge-carrier mobilities observed in many DLCs³ and their self-healing properties are among the most remarkable characteristics of these systems. DLC materials with

high 1D charge carrier mobility along columnar superstructures show potential as active components in organic electronics,⁴ whereby the control of their molecular packing and long-range organization through the design of the building block represents a prime concern for the performance in devices. In this context, the uniaxial alignment with edge-on orientation of the molecules and columns parallel to the substrate is needed for field-effect transistors (FETs) to ensure charge migration between the source and the drain electrodes, while the homeotropic alignment with a face-on orientation of the discs and the columnar axes perpendicular to the substrate is expected to be beneficial to the performance in photovoltaic cells (PVCs) and light-emitting diodes (LEDs).⁵ The unique properties of such

*Authors to whom correspondence should be addressed. E-mail: chmcc@nus.edu.sg (C.C.), chmwuj@nus.edu.sg (J.W.).

- (1) (a) Lehn, J.-M. *Supramolecular Chemistry: Concepts and Perspectives*; Wiley-VCH: Weinheim, Germany, 1995. (b) James, D. K.; Tour, J. M. In *Nanoscale Assembly Techniques*; Huck, W. T. S., Ed.; Springer: New York, 2005. (c) Hirst, A. R.; Escuder, B.; Miravet, J. F.; Smith, D. K. *Angew. Chem. Int. Ed.* **2008**, *47*, 8002.
- (2) Chandrasekhar, S.; Sadashiva, B. K.; Suresh, K. A. *Pramana* **1977**, *9*, 471.
- (3) (a) Adam, D.; Schuhmacher, P.; Simmerer, J.; Haussling, L.; Siemensmeyer, K.; Etbach, K. H.; Ringsdorf, H.; Haarer, D. *Nature* **1994**, *371*, 141. (b) van de Craats, A. M.; Warman, J. M.; Fechtenkötter, A.; Brand, J. D.; Harbison, M. A.; Müllen, K. *Adv. Mater.* **1999**, *11*, 1469. (c) Watson, M. D.; Fechtenkötter, A.; Müllen, K. *Chem. Rev.* **2001**, *101*, 1267. (d) Bushby, R. J.; Lozman, O. R. *Curr. Opin. Solid State Mater. Sci.* **2002**, *6*, 569. (e) Simpson, C. D.; Wu, J.-S.; Watson, M. D.; Müllen, K. *J. Mater. Chem.* **2004**, *14*, 494. (f) Sergeev, S.; Pisula, W.; Geerts, Y. H. *Chem. Soc. Rev.* **2007**, *36*, 1902. (g) Wu, J.-S.; Pisula, W.; Müllen, K. *Chem. Rev.* **2007**, *107*, 718. (h) Demus, D.; Goodby, J.; Gray, G. W.; Spiess, H.-W.; Vill, V.; Chandrasekhar, S. *Handbook of Liquid Crystals*; Wiley-VCH: Weinheim, Germany, 2008; p 749.
- (4) (a) Struijk, C. W.; Sieval, A. B.; Dakhorst, J. E. J.; Kimkes, P.; Koehorst, R. B. M.; Donker, H.; Schaafsma, T. J.; Picken, S. J.; van de Craats, A. M.; Warman, J. M.; Zuilhof, H.; Sudhölter, E. J. R. *J. Am. Chem. Soc.* **2000**, *122*, 11057. (b) Schmidt-Mende, L.; Fechtenkötter, A.; Müllen, K.; Moons, E.; Friend, R. H.; MacKenzie, J. D. *Science* **2001**, *293*, 1119. (c) van de Craats, A. M.; Stutzmann, N.; Bunk, O.; Nielsen, M. M.; Watson, M.; Müllen, K.; Chanzy, H. D.; Siringhaus, H.; Friend, R. H. *Adv. Mater.* **2003**, *15*, 495. (d) Schmidtke, J. P.; Friend, R. H.; Kastler, M.; Müllen, K. *J. Chem. Phys.* **2006**, *124*, 17.
- (5) (a) Stapff, I. H.; Stumppfen, V.; Wendorff, J. H.; Spohn, D. B.; Mobius, D. *Liq. Cryst.* **1997**, *23*, 613. (b) Zucchi, G.; Donnio, B.; Geerts, Y. H. *Chem. Mater.* **2005**, *17*, 4273. (c) Pisula, W.; Menon, A.; Setpputat, M.; Lieberwirth, I.; Kolh, U.; Tracz, A.; Siringhaus, H.; Pakula, T.; Müllen, K. *Adv. Mater.* **2005**, *17*, 684. (d) Breiby, D. W.; Bunk, O.; Pisula, W.; Sølling, T. I.; Tracz, A.; Pakula, T.; Müllen, K.; Nielsen, M. M. *J. Am. Chem. Soc.* **2005**, *127*, 11288.

superstructures—namely, anisotropic conduction of charge carriers in the nanodimension—make them especially interesting from the point of view of the emerging field of supramolecular electronics.⁶ Their liquid crystallinity provides unique mechanical properties and allows the molecules enough motional freedom to self-heal possible defects along the conducting channels. Furthermore, their optical and mesomorphic properties can be tailored by varying the nature of the central core and the peripheral substituent. While the lateral chains are certainly of importance in establishing the liquid crystalline behavior, charge transport properties are primarily determined by the aromatic character of the cores and the interactions among them.⁷

Generally, columnar mesophases are generated from disklike molecules. A large number of DLCs are known and derived from more than 50 different mesogens, typically being a polyaromatic core such as triphenylene (TP),⁸ phthalocyanine,⁹ and hexabenzocoronene (HBC).¹⁰ The ether- and thioether-substituted triphenylene derivatives (e.g., **TPC6** in Figure 1)¹¹ are among the

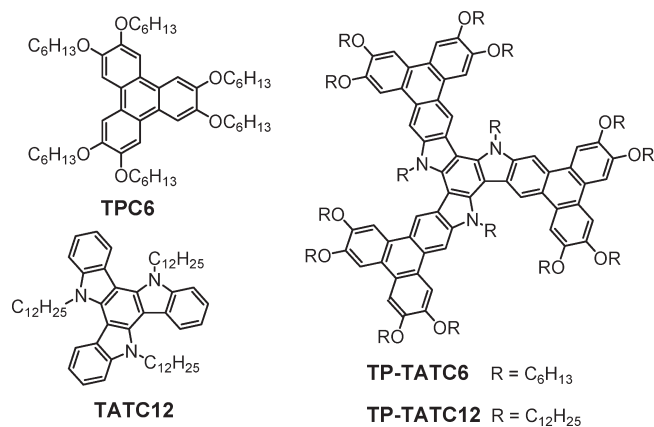


Figure 1. Molecular structures of **TPC6**, **TATC12**, **TP-TATC6**, and **TP-TATC12**.

most widely investigated DLCs, and various methods have been developed to synthesize this type of molecule.¹² TP and its derivatives have been known as hole-transporting materials, and their photoinduced charge-carrier mobilities ranged from 10^{-5} $\text{cm}^2 \text{V}^{-1} \text{s}^{-1}$ in the isotropic phase to 10^{-1} $\text{cm}^2 \text{V}^{-1} \text{s}^{-1}$ in highly ordered discotic mesophases.¹³ It has been shown that, for TP derivatives, a helical arrangement of discotic molecules results in significantly improved intracolumnar packing and high charge-carrier mobilities.^{3a,14} In addition, a wide range of TP-containing liquid-crystalline polymers,¹⁵ elastomers,¹⁶ networks,¹⁷ and partially fluorinated¹⁸ and amphiphilic¹⁹ TP compounds have been reported and used for different purposes. With very few exceptions,²⁰ most of the systems containing two or more TPs have a structural feature that the TP units are linked to each

- (6) Hoeben, F. J. M.; Jonkheijm, P.; Meijer, E. W.; Schenning, A. P. H. *J. Chem. Rev.* **2005**, *105*, 1491.
- (7) (a) Cornil, J.; Lemaury, V.; Calbert, J.-P.; Brédas, J.-L. *Adv. Mater.* **2002**, *14*, 726. (b) Senthilkumar, K.; Grozema, F. C.; Bickelhaupt, F. M.; Siebbeles, L. D. A. *J. Chem. Phys.* **2003**, *119*, 9809. (c) Gearba, R. I.; Lehmann, M.; Levin, J.; Ivanov, D. A.; Koch, M. H. J.; Barbera, J.; Debije, M. G.; Piris, J.; Geerts, Y. H. *Adv. Mater.* **2003**, *15*, 1614. (d) Palma, M.; Levin, J.; Lemaury, V.; Liscio, A.; Palermo, V.; Cornil, J.; Geerts, Y. H.; Lehmann, M.; Samori, P. *Adv. Mater.* **2006**, *18*, 3313. (e) Coropceanu, V.; Cornil, J.; da Silva Filho, D. A.; Olivier, Y.; Silbey, R.; Brédas, J.-L. *Chem. Rev.* **2007**, *107*, 926.
- (8) (a) Perez, D.; Guitian, E. *Chem. Soc. Rev.* **2004**, *33*, 274. (b) Sarhan, A. A. O.; Bolm, C. *Chem. Soc. Rev.* **2009**, *28*, 2730. (c) Kumar, S. *Liq. Cryst.* **2004**, *31*, 1037.
- (9) (a) Tant, J.; Geerts, Y. H.; Lehmann, M.; De Cupere, V.; Zucchi, G.; Laursen, B. W.; Bjornholm, T.; Lemaury, V.; Marcq, V.; Burquel, A.; Hennebicq, E.; Gardebien, F.; Viville, P.; Beljonne, D.; Lazzaroni, R.; Cornil, J. *J. Phys. Chem. B* **2006**, *110*, 3449. (b) Atilla, D.; Kilinc, N.; Yuksel, F.; Gurek, A. G.; Ozturk, Z. Z.; Ahsen, V. *Synth. Met.* **2009**, *159*, 13.
- (10) (a) Herwig, P.; Kayser, C. W.; Müllen, K.; Spiess, H. W. *Adv. Mater.* **1996**, *8*, 510. (b) Wu, J.-S.; Watson, M. D.; Zhang, L.; Wang, Z.-H.; Müllen, K. *J. Am. Chem. Soc.* **2004**, *126*(1), 177. (c) Pisula, W.; Kastler, M.; Wasserfallen, D.; Pakula, T.; Müllen, K. *J. Am. Chem. Soc.* **2004**, *126*, 8074. (d) Wang, Z.-H.; Watson, M. D.; Wu, J.-S.; Müllen, K. *Chem. Commun.* **2004**, 336. (e) Wasserfallen, D.; Fischbach, I.; Chebotareva, N.; Kastler, M.; Pisula, W.; Jäckel, F.; Watson, M. D.; Schnell, I.; Rabe, J. P.; Spiess, H. W.; Müllen, K. *Adv. Funct. Mater.* **2005**, *15*, 1585.
- (11) (a) Boden, N.; Borner, R. C.; Bushby, R. J.; Cammidge, A. N.; Jesudason, M. V. *Liq. Cryst.* **1993**, *15*, 851. (b) Schulte, J. L.; Laschat, S.; Vill, V.; Nishikawa, E.; Finkelmann, H.; Nimitz, M. *Eur. J. Org. Chem.* **1998**, 2499. (c) Kumar, S.; Varshney, S. K. *Synthesis* **2001**, 305. (d) Kumar, S. *Chem. Soc. Rev.* **2006**, *35*, 83. (e) Laschat, S.; Baro, S. A.; Steinke, N.; Giesselmann, F.; Hgele, C.; Scalia, G.; Judele, R.; Kapatsina, E.; Sauer, S.; Schreivogel, A.; Tosoni, M. *Angew. Chem., Int. Ed.* **2007**, *46*, 4832.
- (12) (a) Naarmann, H.; Hanack, M.; Mattmer, R. *Synthesis* **1994**, 477. (b) Kumar, S.; Manickam, M. *Chem. Commun.* **1997**, 1615. (c) Boden, N.; Bushby, R. J.; Lu, Z.; Headdock, G. *Tetrahedron Lett.* **2000**, *41*, 10117. (d) Kumar, S. *Liq. Cryst.* **2005**, *32*, 1089.
- (13) (a) Adam, D.; Haarer, D.; Closs, F.; Funhoff, D.; Siemsmeyer, K.; Schuhmacher, P.; Ringsdorf, H.; Bunsenges, B. *Phys. Chem.* **1993**, *97*, 1366. (b) Adam, D.; Schuhmacher, P.; Simmerer, J.; Maubling, L.; Paulus, W.; Siemsmeyer, K.; Eitzbach, K. H.; Ringsdorf, H.; Haarer, D. *Adv. Mater.* **1995**, *7*, 276. (c) Simmerer, J.; Glusen, B.; Paulus, W.; Kettner, A.; Schuhmacher, P.; Adam, D.; Eitzbach, K. H.; Siemsmeyer, K.; Wendorff, J. H.; Ringsdorf, H.; Haarer, D. *Adv. Mater.* **1996**, *8*, 815. (d) Christ, T.; Glusen, B.; Greiner, A.; Kettner, A.; Sander, R.; Stumpf, V.; Tsukruk, V.; Wendorff, J. H. *Adv. Mater.* **1997**, *9*, 48. (e) Christ, T.; Stumpf, V.; Wendorff, J. H. *Makromol. Chem. Rapid. Commun.* **1997**, *18*, 93.
- (14) (a) Adam, D.; Closs, F.; Frey, T.; Funhoff, D.; Haarer, D.; Ringsdorf, H.; Schuhmacher, P.; Siemsmeyer, K. *Phys. Rev. Lett.* **1993**, *70*, 457. (b) Bengs, H.; Closs, F.; Frey, T.; Funhoff, D.; Ringsdorf, H.; Siemsmeyer, K. *Liq. Cryst.* **1993**, *15*, 565. (c) Haarer, D.; Adam, D.; Simmerer, J.; Closs, F.; Funhoff, D.; Hussling, L.; Siemsmeyer, K.; Ringsdorf, H.; Schumacher, P. *Mol. Cryst. Liq. Cryst.* **1994**, *252*, 155. (d) Mizoshita, N.; Monobe, H.; Inoue, M.; Ukon, M.; Watanabe, T.; Shimizu, Y.; Hanabusa, K.; Kato, T. *Chem. Commun.* **2002**, 428.
- (15) (a) Cui, L.; Miao, J.; Zhu, L. *Macromolecules* **2006**, *39*, 2536. (b) Zhang, C.; He, Z.; Mao, H.; Wang, J.; Wang, D.; Wang, Y.; Li, Z.; Pu, J. *J. Lumin.* **2007**, *122–123*, 931.
- (16) (a) Closs, F.; Haussling, L.; Henderson, P.; Ringsdorf, H.; Schuhmacher, P. *J. Chem. Soc. Perkin Trans. 1* **1995**, *7*, 829. (b) Talroze, R. V.; Otmakhova, O. A.; Koval, M. A.; Kuptsov, S. A.; Plate, N. A.; Finkelmann, H. *Macromol. Chem. Phys.* **2000**, *201*(8), 877. (c) Bushby, R. J.; Lozman, O. R. *Curr. Opin. Colloid Interface Sci.* **2002**, *7*, 343.
- (17) (a) Hirai, Y.; Monobe, H.; Mizoshita, N.; Moriyama, M.; Hanabusa, K.; Shimizu, Y.; Kato, T. *Adv. Funct. Mater.* **2008**, *18*, 1668. (b) Shen, Z.; Yamada, M.; Miyake, M. *J. Am. Chem. Soc.* **2007**, *129*, 14271. (c) Gupta, S. K.; Raghunathan, V. A.; Sandeep, K. *New J. Chem.* **2009**, *33*, 112. (d) Zelcer, A.; Donnio, B.; Bourgogne, C.; Cukiernik, F. D.; Guillon, D. *Chem. Mater.* **2007**, *19*, 1992.
- (18) (a) Dahn, U.; Erdelen, C.; Ringsdorf, H.; Festag, R.; Wendorff, J. H.; Heiney, P. A.; Maliszewski, N. C. *Liq. Cryst.* **1995**, *19*, 759. (b) Terasawa, N.; Monobe, H.; Shimizu, Y. *Chem. Lett.* **2003**, *32*, 214.
- (19) (a) Boden, N.; Bushby, R. J.; Jesudason, M. V.; Sheldrick, B. *J. Chem. Soc., Chem. Commun.* **1988**, 1342. (b) Barberá, J.; Garcés, A. C.; Jayaraman, N.; Omenat, A.; Serrano, J. L.; Stoddart, J. F. *Adv. Mater.* **2001**, *13*, 175. (c) Tao, K.; Wang, Y.-X.; Wang, W.-D.; Lu, D.-R.; Wang, Y.; Bai, R.-K. *Macromol. Chem. Phys.* **2009**, *210*, 478. (d) Wang, D.-G.; Hsu, J. F.; Bagui, M.; Dusevich, V.; Wang, Y.; Liu, Y.; Holder, A. J.; Peng, Z.-H. *Tetrahedron Lett.* **2009**, *50*, 2147.
- (20) Sandeep, K.; Varshney, S. K. *Org. Lett.* **2002**, *4*, 157.

other via soft chains to form self-assembled superstructures.²¹

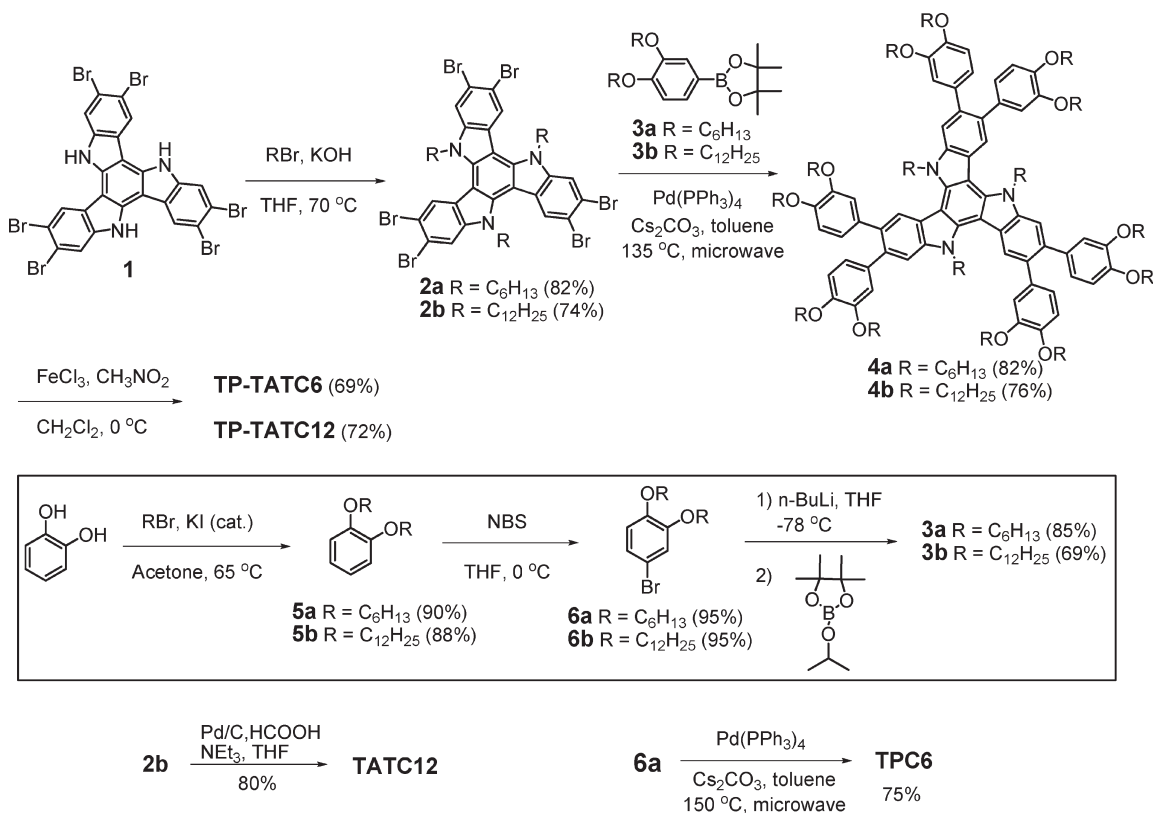
To achieve high charge-carrier mobility, it is essential to control the molecular order of the discotic molecules in macroscopic thin films either by structural design or by physical processing. It is supposed that DLCs with large rigid cores form highly ordered columnar structures because of enhanced π - π interactions between aromatic cores.^{3g} Thus, the design of new large π -conjugated mesogens with high molecular order represents one of the major tasks of the area. One general approach is to expand the core size of polycyclic aromatic hydrocarbons (PAHs) from TP to larger-sized discs such as hexabenzocoronenes.¹⁰ However, further expansion of the disk core usually requires multiple-step synthesis and tedious purification, and sometimes it also encounters solubility problems that arise from the strong intermolecular π -stacking.²²

Another important issue for practical device applications using DLCs is the intrinsic electronic properties of the π -conjugated mesogens. Depending on the ionization potential (i.e., the energy level of the highest occupied molecular orbital (HOMO)) or electron affinity (i.e., the energy level of the lowest unoccupied molecular orbital (LUMO)), the discotic molecule prefers to transport either positive holes or negative electrons, and accordingly, the materials can be classified as *p*-type or *n*-type semiconductors. Usually, most PAH-based DLCs prefer to transport holes and, thus, they can serve as typical *p*-type semiconductors.²³ On the other hand, when electron-withdrawing groups are attached to PAHs or high-electron-affinity heteroaromatics are included in the core, the discotic molecules show *n*-type character.²⁴ The energy levels of frontier molecular orbitals of a discotic molecule also determine the hole or electron injection barrier at the interface of the metal electrode in electronic devices. Moreover, they also affect the chemical stability of the materials because too-high-lying HOMO energy levels will lead to easy oxidation, whereas too-low-lying LUMO energy levels will result in fast reduction reactions. Therefore, tuning of the electronic properties through control of π -conjugation or substitution is also a crucial issue in the design of DLC materials.

In search of efficient hole-transporting semiconductors, carbazole-based oligomers and polymers have been shown to be excellent candidates, because of their high chemical stability²⁵ and hole-transporting nature,²⁶ and their applications for photorefractive materials,²⁷ solar cells,²⁸ and organic LEDs²⁹ have been reported. A recent interest is to include carbazole units into discotic mesogens, so that both the hole-transporting properties and the supramolecular organization associated with DLCs can be utilized. A successful example is triazatruxene (TAT), which is a disklike molecule with *C*₃ symmetry that can be considered as an extended π -system in which three carbazole units share one aromatic ring (see Figure 1).³⁰ The structural resemblance with the well-known hole transporter carbazole, together with the π -extended structure, renders TATs as attractive candidates as charge-transporting materials in organic electronic devices. Surprisingly, while its all-carbon counterpart truxene has been extensively investigated for the construction of extended hydrocarbons,³¹ electro-optical devices,³² or liquid crystals,³³ the studies on TAT-based materials are quite limited.³⁴ Recent reports showed that substitution at the peripheries and/or the -NH sites by flexible chains afforded liquid crystalline property of this disklike molecule and the obtained materials also

- (21) Lee, J.-H.; Choi, S.-M.; Pate, B. D.; Chisholm, M. H.; Han, Y.-S. *J. Mater. Chem.* **2006**, *16*, 2785.
- (22) (a) Simpson, C. D.; Brand, J. D.; Berresheim, A. J.; Przybilla, L.; Räder, H. J.; Müllen, K. *Chem.—Eur. J.* **2002**, *8*, 1424. (b) Wu, J.-S.; Gherghel, L.; Watson, M. D.; Li, J.; Wang, Z.-H.; Simpson, C. D. M.; Kolb, U.; Müllen, K. *Macromolecules* **2003**, *36*, 7082. (c) Wu, J.-S.; Tomović, Z.; Enkelmann, V.; Müllen, K. *J. Org. Chem.* **2004**, *69*, 5179.
- (23) (a) Weidkamp, K. P.; Afzali, A.; Tromp, R. M.; Hamers, R. J. *J. Am. Chem. Soc.* **2004**, *126*, 12740. (b) Guo, X.-F.; Myers, M.; Xiao, S.-X.; Lefenfeld, M.; Steiner, R.; Tulevski, G. S.; Tang, J.-Y.; Baumert, J.; Leibfarth, F.; Yardley, J. T.; Steigerwald, M. L.; Kim, P.; Nuckolls, C. *Proc. Natl. Acad. Sci., U.S.A.* **2006**, *103*, 11452. (c) Natsume, Y.; Minakata, T.; Aoyagi, T. *Thin Solid Films* **2009**, *517*, 3005.
- (24) (a) Ahrens, M. J.; Fuller, M. J.; Wasielewski, M. R. *Chem. Mater.* **2003**, *15*, 2684. (b) Sakamoto, Y.; Suzuki, T.; Kobayashi, M.; Gao, Y.; Fukai, Y.; Inoue, Y.; Tokito, S. *J. Am. Chem. Soc.* **2004**, *126*, 8138. (c) Khavryuchenko, V. D.; Khavryuchenko, O. V.; Tarasenko, Y. A.; Lisnyak, V. V. *Chem. Phys.* **2008**, *352*, 231. (d) Li, Y.; Tan, L.; Wang, Z.-H.; Qian, H.-L.; Shi, Y.-B.; Hu, W.-P. *Org. Lett.* **2008**, *10*, 529. (e) Qian, H.-L.; Negri, F.; Wang, C.-R.; Wang, Z.-H. *J. Am. Chem. Soc.* **2008**, *130*, 17970.
- (25) (a) Kuwabara, Y.; Ogawa, H.; Inada, H.; Nona, N.; Shirota, Y. *Adv. Mater.* **1994**, *6*, 667. (b) O'Brien, D. F.; Burrows, P. E.; Forrest, S. R.; Koene, B. E.; Loy, D. E.; Thompson, M. E. *Adv. Mater.* **1998**, *10*, 1108. (c) Koene, B. E.; Loy, D. E.; Thompson, M. E. *Chem. Mater.* **1998**, *10*, 2235. (d) Thomas, K. R. J.; Lim, J. T.; Tao, Y. T.; Ko, C. W. *J. Am. Chem. Soc.* **2001**, *123*, 9404. (e) Li, J.; Liu, D.; Li, Y.; Lee, C. S.; Kwong, H. L.; Lee, S. *Chem. Mater.* **2005**, *17*, 1208.
- (26) (a) Shirota, Y. *J. Mater. Chem.* **2000**, *10*, 1. (b) Brunner, K.; Dijken, A. V.; Börner, H.; Bastiaansen, J. J. A. M.; Kiggen, N. M. M.; Langeveld, B. M. W. *J. Am. Chem. Soc.* **2004**, *126*, 6035. (c) Romero, D. B.; Schaefer, M.; Leclerc, M.; Adès, D.; Siove, A.; Zuppiroli, L. *Synth. Met.* **1996**, *80*, 271. (d) Justin Thomas, K. R.; Lin, J. T.; Tao, Y.-T.; Ko, C.-W. *J. Am. Chem. Soc.* **2001**, *123*, 9404. (e) Shirota, Y.; Kageyama, H. *Chem. Rev.* **2007**, *107*, 953.
- (27) (a) Kippelen, B.; Marder, S. R.; Hendrickx, E.; Maldonado, J. L.; Guillemet, G.; Volodin, B. L.; Steele, D. D.; Enami, Y.; Sandalphon; Yao, Y.-J.; Wang, J.-F.; Rockel, H.; Erskine, L.; Peyghambarian, N. *Science* **1998**, *279*, 54. (b) Wright, D.; Gubler, U.; Roh, Y.; Moerner, W. E.; He, M.; Twieg, R. J. *Appl. Phys. Lett.* **2001**, *79*, 4274.
- (28) (a) Blouin, N.; Michaud, A.; Leclerc, M. *Adv. Mater.* **2007**, *19*, 2295. (b) Blouin, N.; Michaud, A.; Gendron, D.; Wakim, S.; Blair, E.; Neagu-Plesu, R.; Belletete, M.; Durocher, G.; Tao, Y.; Leclerc, M. *J. Am. Chem. Soc.* **2008**, *130*, 732. (c) Wang, Z.-S.; Koumura, N.; Cui, Y.; Takahashi, M.; Sekiguchi, H.; Mori, A.; Kubo, T.; Furube, A.; Hara, K. *Chem. Mater.* **2008**, *20*, 3993.
- (29) (a) Wang, Y.-Z.; Epstein, A. J. *Acc. Chem. Res.* **1999**, *32*, 217. (b) Grazulevicius, J. V.; Strohriegel, P.; Pielichowski, J.; Pielichowski, K. *Prog. Polym. Sci.* **2003**, *28*, 1297. (c) Morin, J.-F.; Leclerc, M.; Adès, D.; Siove, A. *Macromol. Rapid Commun.* **2005**, *26*, 761. (d) Blouin, N.; Leclerc, M. *Acc. Chem. Res.* **2008**, *41*, 1110.
- (30) Robertson, N.; Parsons, S.; MacLean, E. J.; Coxalland, R. A.; Mount, A. R. *J. Mater. Chem.* **2000**, *10*, 2043.
- (31) (a) Gómez-Lor, B.; González-Cantalapiedra, E.; Ruiz, M.; de Frutos, O.; Cárdenas, D. J.; Santos, A.; Echavarren, A. M. *Chem.—Eur. J.* **2004**, *10*, 2601. (b) Peng, Q.; Xu, J.; Li, M.-J.; Zheng, W.-X. *Macromolecules* **2009**, *42*, 5478.
- (32) Sun, Y.; Xiao, K.; Liu, Y.; Wang, J.; Pei, J.; Zhu, D.-B. *Adv. Funct. Mater.* **2005**, *15*, 818.
- (33) Perova, T. S.; Vij, J. K. *Adv. Mater.* **1995**, *7*, 919.
- (34) (a) Gómez-Lor, B.; Echavarren, A. M. *Org. Lett.* **2004**, *6*, 2993. (b) Gómez-Lor, B.; Hennrich, G.; Alonso, B.; Monge, A.; Gutierrez-Puebla, E.; Echavarren, A. M. *Angew. Chem., Int. Ed.* **2006**, *45*, 4491. (c) Lai, W.-Y.; Chen, Q.-Q.; He, Q.-Y.; Fan, Q.-L.; Huang, W. *Chem. Commun.* **2006**, 1959. (d) Lai, W.-Y.; He, Q.-Y.; Zhu, R.; Chen, Q.-Q.; Huang, W. *Adv. Funct. Mater.* **2008**, *18*, 265. (e) Lai, W.-Y.; Xia, R.-D.; He, Q.-Y.; Levermore, P. A.; Huang, W.; Bradley, D. D. C. *Adv. Mater.* **2009**, *21*, 355.

Scheme 1. Synthesis of TP-TATC6, TP-TATC12, TATC12, and TPC6



exhibited highly ordered self-assembly and high hole mobilities (up to $0.1 \text{ cm}^2 \text{ V}^{-1} \text{ s}^{-1}$).³⁵

To further control the self-assembly and electronic properties of this type of promising material, herein we design a new largely extended π -system in which three TP units are fused together with a TAT core by sharing three benzene rings (see Figure 1). Such a design is supposed to combine the self-assembling and hole-transporting properties of both TAT and TP mesogens and, thus, new interesting properties are expected from this type of material. The largely expanded core size is believed to be able to enhance the intermolecular interactions and the attachment of different alkyl chains can tune their solubility and thermal properties. The discotic molecules attached by *n*-hexyl or *n*-dodecyl chains are referred to as **TP-TATC6** and **TP-TATC12**, respectively. In this article, we report the success synthesis of this type of discotic mesogen by efficient coupling reactions and cyclization reactions. Their photophysical properties in solution and in thin films were investigated by ultraviolet–visible (UV–vis) absorption and fluorescence spectroscopy. Their electronic properties were probed by cyclic voltammetry. Their thermal behavior and self-assembly in bulk state were studied in details by different techniques such thermogravimetric analysis (TGA), differential scanning calorimetry (DSC), polarized optical microscopy (POM), and X-ray diffraction (XRD). Their

charge transport property was studied by space-charge limited-current (SCLC) technique. In addition, an unusual phenomenon was observed for one of these molecules (**TP-TATC12**), which can form physical gel in many solvents without any assistance of hydrogen bonding.

Results and Discussion

Material Synthesis and Characterization. The synthetic route of these large disklike molecules is shown in Scheme 1. The synthesis started from alkylation of the known hexabromotriazatruxene **1**³⁰ to give the compounds **2a** and **2b**, in 82% and 74% yield, respectively. The reaction was done under basic conditions with KOH as the base, and different alkyl chains (i.e., *n*-hexyl and *n*-dodecyl) were attached to the –NH site to increase the solubility and also to tune the thermal behavior of the final compounds. In addition, such *N*-alkylation is also necessary prior to the subsequent Suzuki coupling reactions, because of the poor chemical stability of **1** under the coupling reaction conditions. Compound **2a** (**2b**) then underwent 6-fold Suzuki coupling reactions with the 3,4-dialkoxyphenyl pinacolboronic ester **3a** (**3b**) under microwave irradiation conditions to afford the corresponding 6-fold substituted TAT **4a** (**4b**) in high yields. The 6-fold Suzuki coupling reaction is challenging, because we found that, under conventional heating conditions, in the presence of $\text{Pd(PPh}_3)_4$ and base (aqueous K_2CO_3),³⁶ at least two days were required, because of the incomplete

(35) (a) Talarico, M.; Termine, R.; García-Frutos, E. M.; Omenat, A.; Serranoc, J.-L.; Gómez-Lor, B.; Golemme, A. *Chem. Mater.* **2008**, *20*, 6589. (b) Garça-Frutos, E. M.; Gómez-Lor, B. *J. Am. Chem. Soc.* **2008**, *130*, 9173. (c) Gómez-Lor, B.; Alonso, B.; Omenat, A.; Serranoc, J.-L. *Chem. Commun.* **2006**, 5012.

(36) (a) Louie, J.; Hartwig, J. F. *Tetrahedron Lett.* **1995**, *36*, 3609. (b) Miyaura, N.; Suzuki, A. *Chem. Rev.* **1995**, *95*, 2457. (c) Yin, L.-X.; Liebscher, J. *Chem. Rev.* **2007**, *107*, 133.

couplings and the products can only be obtained in low yields (< 30%) after tedious purification. Therefore, the reaction was conducted under a microwave-assisted condition, which is known to be a very good tool for many palladium-catalyzed C–C coupling reactions.³⁷ Under optimized conditions, i.e., the reaction mixture was conducted in toluene at 135 °C under 100 W of microwave irradiation for 30 min, compounds **4a** and **4b** were obtained in high yields after simple purification by column chromatography. Such microwave-irradiation-accelerated multiple transition-metal-catalyzed coupling reactions were also reported for the synthesis of some star-shaped compounds.^{33,38} The advantages of microwave-assisted heating over the traditional heating conditions lie on, that under microwave irradiation, the energy can be applied directly to the reactants and solvent, rather than conductively via a vessel. Our results again demonstrated that microwave heating was a convenient and powerful technology for preparing star-shaped or multiple branched molecules. The synthesis of the intermediate compounds 3,4-dialkoxyphenyl pinacolboronic ester **3a** and **3b** is also shown in Scheme 1. The catechol was first alkylated with 1-bromohexane and 1-bromododecane to give the respective compounds **5a** and **5b** in high yields. Regio-selective bromination of **5a** and **5b** with *N*-bromosuccinimide (NBS) afforded the corresponding bromides **6a** and **6b** both in 95% yield. The pinacolboronic esters **3a** and **3b** were then prepared by lithiation of **6a** and **6b** with *n*-BuLi, followed by quenching with 2-isopropoxy-4,4',5,5'-tetramethyl-1,3,2-dioxaborolane (1.1 equiv) at –78 °C in good yields.³⁹

The target compounds **TP-TATC6** and **TP-TATC12** were finally obtained by successful intramolecular oxidative cyclodehydrogenation of **4a** and **4b** with FeCl₃ in dichloromethane (DCM), in 69% and 72% yield, respectively. It is known that many PAHs such as hexa-*peri*-hexabenzocoronene can be prepared by FeCl₃-mediated cyclodehydrogenation of appropriate branched oligophenylene precursors where FeCl₃ serves as both an oxidant and a Lewis acid.⁴⁰ Such methods also were used for the synthesis of some sulfur-containing polycyclic aromatics.⁴¹ Herein, this method was again used for the

cyclization of **4a** and **4b**, and the desired discotic molecules were obtained in high yields after simple purification by column chromatography. We also optimized the reaction conditions by examining the amount and the speed of FeCl₃ added, as well as the reaction temperature. To avoid any possible side reactions such as chlorination and dealkylation,⁴⁰ the reaction was done at 0 °C with nitrogen gas purging through the reaction solution during the entire reaction period. It was determined that the reaction was completed within < 30 min and even in the presence of an excess amount of FeCl₃ (more than 4 equiv per newly formed C–C bond), no chlorinated byproducts were generated and no dealkylation were observed. It should be mentioned that the choice of 3,4-dialkoxyphenyl groups also help to conduct a regioselective cyclization, i.e., only the active sites at the 6-position participated in the C–C bond formation and no isomers were observed in the obtained **TP-TATC6** and **TP-TATC12**. Both final compounds can be readily dissolved in common organic solvents such as DCM, CHCl₃, toluene and chlorobenzene and these allow us to do conventional characterizations by standard spectroscopic techniques.

The identity and purity of all new compounds were confirmed by ¹H and ¹³C NMR spectra, electron ionization mass spectrometry (EI-MS), matrix-assisted laser desorption ionization time-of-flight mass spectrometry (MALDI-TOF MS), high-resolution EI-MS, and elemental analysis. The ¹H NMR spectra of the **TP-TATC6** and **TP-TATC12** disclose well-resolved resonances that can be assigned to the desired structure (see the Supporting Information). In particular, the resonances in the aromatic range show sharp singlet signals that belong to the TP units and the TAT core with chemical shift obviously downfield shift, in comparison to the respective precursors **4a** and **4b**. Such a downfield shift is due to the shielding of the aromatic protons under the induced magnetic field generated by the ring current of an aromatic π -system. At the same time, the resonances for the methylene units close to the aromatic system (e.g., N–CH₂, O–CH₂) also shift to low field after cyclization reactions. The concentration-dependent ¹H NMR spectra of **TP-TATC6** and **TP-TATC12** were recorded in CDCl₃ at room temperature with concentration varied between 3 mg/mL and 21 mg/mL and no obvious concentration dependence was observed. This suggests that the intermolecular interactions are not strong in dilute chloroform solution, probably because the *N*-alkyl substitution causes steric barrier for the intermolecular association. However, the self-association of these disklike molecules in solutions are strongly dependent on the nature of solvents, and it is very interesting to find that stable transparent gels of **TP-TATC12** can be formed in many nonpolar solvents such as hexane. In addition, ordered self-assembly of these discotic molecules was observed in solid state, and all these will be discussed in detail later in this work.

For comparison, the dodecyl-chain-substituted TAT (**TATC12**, see Figure 1) was also prepared in 80% yield by

- (37) Singh, B. K.; Kaval, N.; Tomar, S.; van der Eycken, E.; Parmar, V. *S. Org. Process Res. Dev.* **2008**, *12*, 468.
(38) (a) Kappe, C. O. *Angew. Chem., Int. Ed.* **2004**, *43*, 6250. (b) De la Hoz, A.; Dkz-Ortiz, A.; Moreno, A. *Chem. Soc. Rev.* **2005**, *34*, 164. (c) Roberts, B. A.; Strauss, C. R. *Acc. Chem. Res.* **2005**, *38*, 653. (d) Leadbeater, N. E. *Chem. Commun.* **2005**, 2881.
(39) (a) Coudret, C. *Synth. Commun.* **1996**, *26*, 3543. (b) Krämer, C. S.; Zimmermann, T. J.; Sailer, M. T.; Müller, J. J. *Synthesis* **2002**, 1163.
(40) (a) Müller, M.; Kübel, C.; Müllen, K. *Chem.—Eur. J.* **1998**, *4*, 2099. (b) Draper, S. M.; Gregg, D. J.; Madathil, R. *J. Am. Chem. Soc.* **2002**, *124*, 3486. (c) Wang, Z.; Tomovi, Ž.; Kastler, M.; Pretsch, R.; Negri, F.; Enkelmann, V.; Müllen, K. *J. Am. Chem. Soc.* **2004**, *126*, 7794. (d) Wu, J.-S.; Tomović, Ž.; Enkelmann, V.; Müllen, K. *J. Org. Chem.* **2004**, *69*, 5179. (e) Wu, J.-S.; Watson, M. D.; Tchebotareva, N.; Wang, Z.-H.; Müllen, K. *J. Org. Chem.* **2004**, *69*, 8194. (f) Cao, X.-Y.; Zhang, W.; Zi, H.; Lu, H.; Pei, J. *J. Org. Chem.* **2005**, *70*, 3645. (g) Zhou, Y.; Liu, W.-J.; Zhang, W.; Cao, X.-Y.; Zhou, Q.; Ma, Y.-G.; Pei, J. *J. Org. Chem.* **2006**, *71*, 6822.
(41) (a) Tovar, J. D.; Rose, A.; Swager, T. M. *J. Am. Chem. Soc.* **2002**, *124*, 7762. (b) Pei, J.; Zhang, W.-Y.; Mao, J.; Zhou, X.-H. *Tetrahedron Lett.* **2006**, *47*, 1551. (c) Wang, J.-Y.; Zhou, Y.; Yan, J.; Ding, L.; Ma, Y.-G.; Cao, Y.; Wang, J.; Pei, J. *Chem. Mater.* **2009**, *21*, 2595.

debromination of **2b** in the presence of Pd/C in THF, according to a reported procedure (Scheme 1).^{34d} Interestingly, we found that, under microwave irradiation at high temperature (150 °C), compound **3a** can be easily converted to the corresponding TP compound **TPC6** in high yield, but this reaction does not work under conventional heating conditions. Such a microwave-assisted cyclotrimerization is very unusual, and a detailed study of the mechanism is undergoing and will not be discussed here. The obtained **TPC6** was also used as a reference for **TP-TATC6** and **TP-TATC12**.

Photophysical Properties. The UV–vis absorption and fluorescence spectra of **TP-TATC6** and **TP-TATC12** were recorded in dilute solutions (1×10^{-6} M) in DCM and in thin films. The spectra for both compounds are almost identical to each other, so only the representative spectra of **TP-TATC6** are shown in Figure 2. For comparison, the absorption and emission spectra of **TPC6**, **TATC12**, and **4a** were also recorded in DCM (see Figure 2) and all of the data are collected in Table 1. Compound **TP-TATC6** in DCM shows an intense absorption band centered at 374 nm ($\log \epsilon = 5.01$, where ϵ represents the molar extinction coefficient in $\text{M}^{-1} \text{cm}^{-1}$), whereas their absorption spectra in the thin film exhibit

long tails at the lower-energy edge, because of aggregation of these disklike molecules in solid state. Its fluorescence spectrum in DCM displays two well-resolved fluorescence bands at ~ 438 nm and ~ 460 nm, together with a shoulder at 470 nm. In thin films, the fluorescence spectrum red-shifts to longer wavelength, with two well-resolved peaks at ~ 450 nm and ~ 475 nm, together with a long tail at the low-energy side, because of enhanced aggregation in the thin film. For comparison, the **TPC6**, **TATC12**, and **4a** exhibit absorption maxima at 278, 316, and 341 nm, and emission maxima at 384, 393, and 420 nm, respectively. Therefore, the larger discotic molecules **TP-TATC6** and **TP-TATC12** show an obvious red-shift, indicating that the fusion of TP moieties onto a TAT core leads to a largely extended π -conjugated system. The optical band gaps of these compounds derived from the onset of their long wavelength absorption spectra in DCM are listed in Table 1 and the **TP-TATC6** has the smallest value of 2.97 eV, whereas **TATC12** and **TPC6** have larger optical band gaps (3.39 and 3.56 eV, respectively). The UV–vis absorption and fluorescence spectra of **TP-TATC6** and **TP-TATC12** were also measured in different solvents, such as hexane, toluene, and THF. It was found that their spectra only showed a slight solvent dependence. The spectra in DCM, THF, and toluene (1×10^{-5} M) are almost identical to each other; however, in the nonpolar hexane, a small bathochromic shift (ca. 3–5 nm) was observed in the fluorescence spectra, compared with those recorded in DCM, indicating a stronger association tendency of these molecules in nonpolar solvents.

Electrochemical Properties. The electrochemical properties of **TP-TATC6**, **TP-TATC12**, **TATC12**, **TPC6**, **4a**, and **4b** were investigated by cyclic voltammetry (CV) in dry DCM with 0.1 M tetrabutylammonium hexafluorophosphate (TBAPF₆) as the supporting electrolyte. The measurement was performed at room temperature with a scan rate of 50 mV/s using a standard three-electrode cell with a platinum wire as the counter electrode, a AgCl/Ag electrode as the reference electrode, and a gold disk electrode as the working electrode. The cyclic voltammograms of these compounds collected from anodic scans are shown in Figure 3 and all potentials are recorded versus AgCl/Ag reference. All these compounds show one

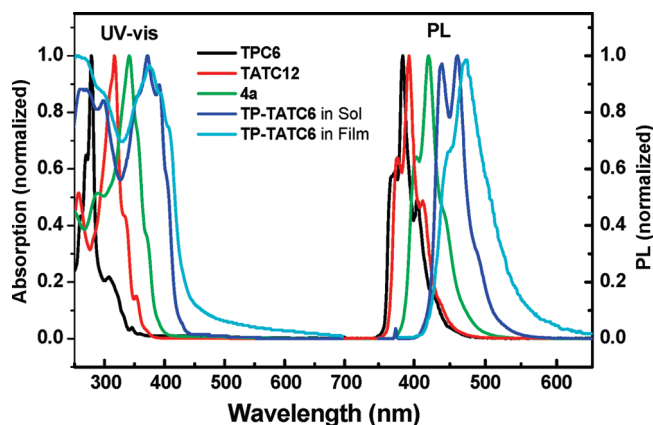


Figure 2. Normalized UV–vis absorption and fluorescence spectra of **TP-TATC6**, **TATC12**, **TPC6**, and **4a** in 1×10^{-6} M DCM solutions. The spectra of **TP-TATC6** were also recorded in thin films prepared by drop casting a 10^{-5} M solution in toluene onto a quartz plate. The fluorescence spectra were recorded upon excitation at the respective absorption maximum wavelength.

Table 1. Summary of Photophysical Properties and Electrochemical Data of Compounds **TPC6**, **TATC12**, **4a**, **TP-TATC6**, and **TP-TATC12**

compound	λ_{ab} [nm]	λ_{em} [nm]	$\log \epsilon_{\text{max}}$ [$\text{M}^{-1} \text{cm}^{-1}$]	Halfwave Potential, $E_{1/2}$ [V]		HOMO [eV]	LUMO [eV]	E_{g} [eV] ^a
				first oxidation wave, $E_{1/2}^{(1)}$	second oxidation wave, $E_{1/2}^{(2)}$			
TPC6	278	384	4.93	1.03		−5.26	−1.70	3.56
TATC12	316	393	4.78	0.77	1.43	−5.02	−1.63	3.39
4a	341	420	4.91	0.73		−4.98	−1.66	3.22
TP-TATC6								
from soln in DCM ^b	374	438, 460	5.01	0.70	1.05	−4.94	−1.97	2.97
from thin film ^c	375	450, 475						
TP-TATC12								
from soln in DCM ^b	372	438, 460	5.12	0.69	1.05	−4.93	−1.96	2.97
from thin film ^c	376	448, 474						

^a Optical band gap estimated from the red edge of the longest wavelength absorption in solution. ^b Data recorded from solution in DCM (1×10^{-6} M). ^c Data recorded from thin film.

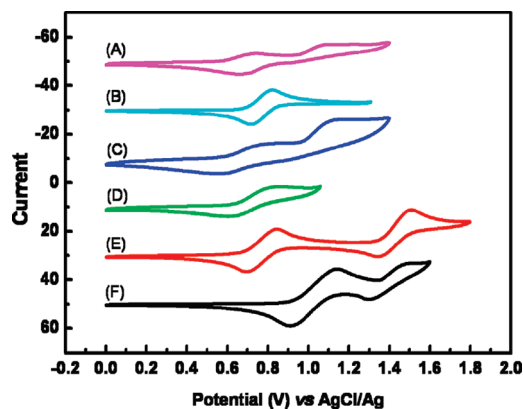


Figure 3. Cyclic voltammograms of TP-TATC12 (curve A), 4b (curve B), TP-TATC6 (curve C), 4a (curve D), TATC12 (curve E), and TPC6 (curve F) in DCM with 0.1 M TBAPF₆ as the supporting electrolyte. A standard three-electrode cell was used with a gold disk as the working electrode, a platinum wire as the counter electrode, and a AgCl/Ag (3 M KCl) as the reference electrode. The concentration of all electroactive substrates is 1 mM, and the scan rate is 50 mV/s.

or two (quasi-) reversible redox waves upon anodic scan; however, there is no obvious redox waves observed during the cathodic scan, indicating the electron-rich and *p*-type character of these TP/TAT-containing systems. Compounds TP-TATC6 and TP-TATC12 exhibit two similar quasi-reversible redox waves with the first and second half-wave potentials ($E_{1/2}^{(1)}$ and $E_{1/2}^{(2)}$, respectively) being ~ 0.69 V and ~ 1.05 V, respectively. The alkylated TAT TATC12 shows two reversible redox waves, with $E_{1/2}^{(1)}$ and $E_{1/2}^{(2)}$ at 0.77 V and 1.43 V, and the alkoxy-chain-substituted TP TPC6 also possess a reversible oxidation wave, with $E_{1/2}^{(1)}$ at 1.03 V. Analysis of these data shows that the first redox wave of the TP-TATC6 and TP-TATC12 can be assigned to the oxidation/reduction of the TAT core, and it also shifts to the lower potential, with respect to that of TATC12, suggesting an extended π -conjugation in the new discotic core molecule. The second redox wave can be correlated to the oxidation/reduction of the TP units; however, it shifts to higher potentials, compared to the TPC6, because of charge repulsion in the oxidized species after the first oxidation of the TAT core. The TAT precursors 4a and 4b show a similar reversible redox wave at $E_{1/2}^{(1)} = 0.77$ V, relative to that of TATC12; however, upon further scanning at high potential, only an irreversible wave was observed, which was likely because oxidative cyclization reactions occurred at high oxidation potentials.

For all CV measurements, the ferrocene/ferrocenium (Fc/Fc⁺) redox couple was used as an internal standard. The energy levels of the HOMO of these electroactive compounds can be derived from the onset of the first oxidation wave, using the following equation: $\text{HOMO} = -(E_{\text{ox}} + 4.8 \text{ eV})$ where E_{ox} is the onset potential of the first oxidation wave versus $E_{\text{Fc}/\text{Fc}^+}$,⁴² and the data are summarized in Table 1. The HOMO

energy levels of TATC12, TPC6, 4a, 4b, TP-TATC6, and TP-TATC12 were then estimated to be -5.02 , -5.26 , -4.98 , -5.02 , -4.94 , and -4.93 eV, respectively. Interestingly, the HOMO energy levels of the expanded core molecules TP-TATC6 and TP-TATC12 match well with the work function of the gold electrode ($w \approx 5.1$ eV),^{35a,43} which is a commonly used electrode in FETs. This character is supposed to ensure efficient hole injection during the operation of a FET device. The LUMO energy levels cannot be determined from the reduction waves; however, it can be estimated from the optical energy gap and the HOMO energy levels by $\text{LUMO} = \text{HOMO} + E_g$ and the data are listed in Table 1.

Thermal Behavior and Self-Assembly under Solid-State Conditions. The thermal behavior and self-assembly of TP-TATC6 and TP-TATC12 in solid state were investigated by different techniques such as TGA, DSC, POM, and variable-temperature XRD (VT XRD). TGA measurements revealed that both compounds were thermally stable with 5% weight loss up to 375 °C under nitrogen (see Figure 4). The DSC curves of TP-TATC6 show two endothermic transitions at 70.8 and 121 °C in the second heating cycle and one exothermic transition at 69.3 °C upon cooling. Similarly, TP-TATC12 show two endothermic transitions at 72.8 and 112.2 °C in the second heating cycle, but there are two exothermic transitions at 104.4 and 59.9 °C upon cooling (see Figure 5).

POM and VT XRD were then used to identify each phase structure. The TP-TATC6 enters an isotropic phase (I) at 122 °C upon heating, as observed by POM measurements. Upon slow cooling, the typical schlieren texture was observed (see Figure 6A), indicating a nematic DLC phase (N_d) below the clearing point. Upon further cooling below 101 °C, a new texture appeared that is typical for columnar liquid crystals (see Figure 6B). Thus, the disklike molecules enter a more-ordered columnar liquid crystalline phase below 101 °C, although this phase transition was not observed in DSC curves, probably because of the small enthalpy change. Upon further cooling to 65 °C, crystalline domains were observed and in each domain, the molecules showed well-ordered alignment (see Figure 6C) that was due to the ordered stacking of these disklike molecules. Thus, the POM clearly revealed phase transitions from a crystalline phase (K) to a columnar crystalline phase (Col), then to a nematic DLC phase (N_d), and finally to an isotropic phase (I) upon heating.

The detailed molecular packing modes of TP-TATC6 in each mesophase were studied by VT XRD. As shown in Figure 7A, the XRD pattern of the pristine powder showed a series of reflection peaks, indicating its crystalline character at room temperature. The reflection peak at 0.345 nm can be correlated to the typical π - π stacking distance in each individual column. In addition, a peak at 0.371 nm was also observed, which is probably correlated to the centroid-to-centroid distance between the neighboring

(42) (a) Pommerehne, J.; Vestweber, H.; Guss, W.; Mahrt, R. F.; Bassler, H.; Porsch, M.; Daub, J. *Adv. Mater.* **1995**, *7*, 551. (b) Sun, Q.-J.; Wang, H.-Q.; Yang, C.-H.; Li, Y.-F. *J. Mater. Chem.* **2003**, *13*, 800.

(43) (a) Rep, D. B. A.; Morpurgo, A. F.; Klapwijk, T. M. *Org. Electr.* **2003**, *4*, 201. (b) Bao, Q.-L.; Lu, Z.-S.; Li, J.; Loh, K. P.; Li, C.-M. *J. Phys. Chem. C* **2009**, *113*, 12530.

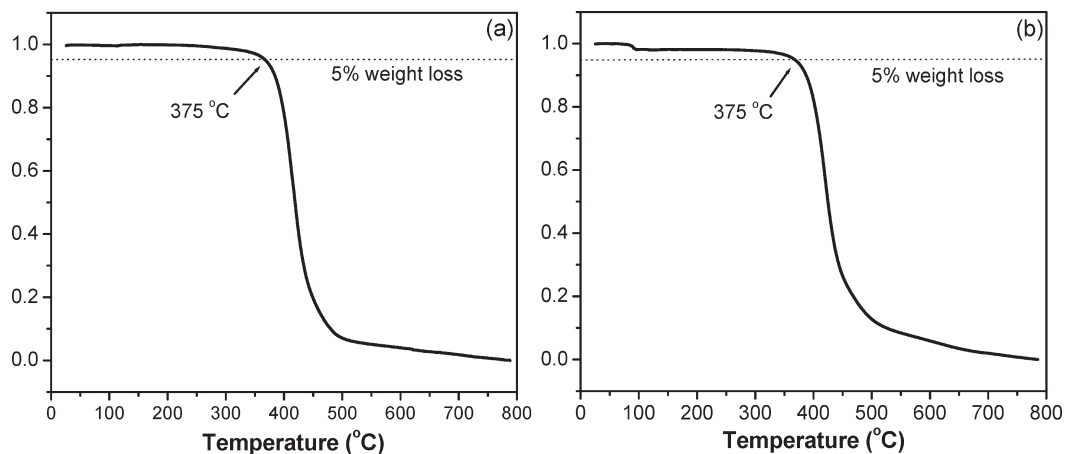


Figure 4. TGA curves of (a) TP-TATC6 and (b) TP-TATC12. The measurements were performed under a nitrogen atmosphere, with heating and cooling rates of 10 °C/min.

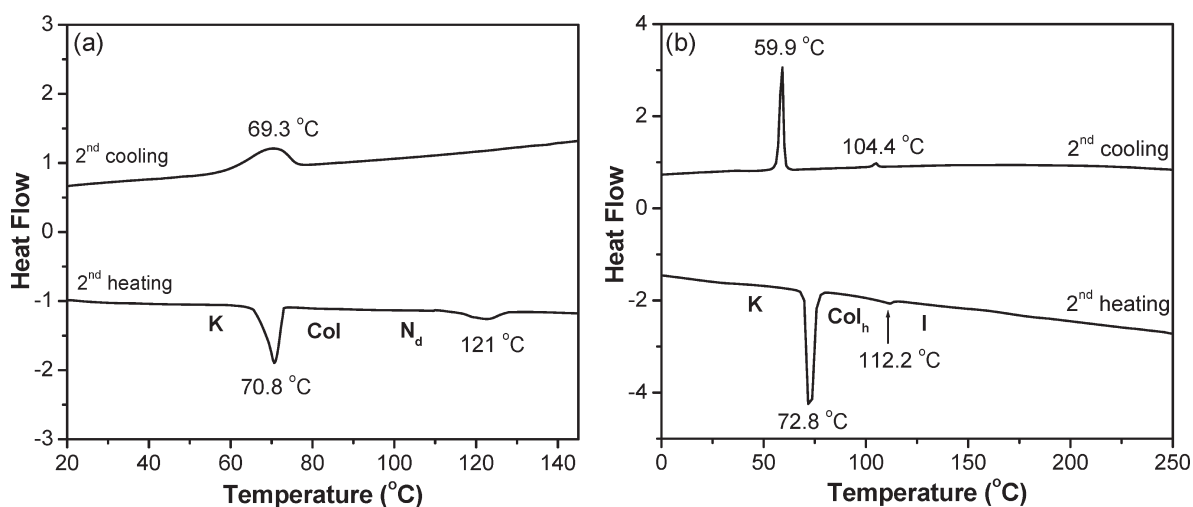


Figure 5. DSC curves of (a) TP-TATC6 and (b) TP-TATC12. The measurements were performed under a nitrogen atmosphere, with heating and cooling rates of 10 °C/min.

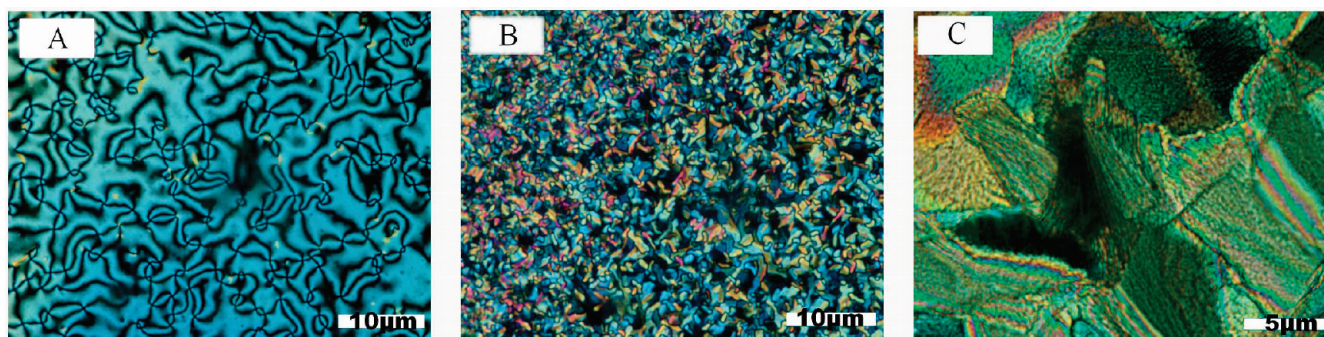


Figure 6. Polarized optical microscopy (POM) images of the drop-casted thin film of TP-TATC6 between two glass slides observed under two crossed polarizers upon slow cooling (1–2 °C/min) from the isotropic phase: (A) at 115 °C, (B) at 75 °C, and (C) at 60 °C.

disks in each tilted column, as previously observed for many DLCs.^{3h,44} However, two-dimensional (2D)

XRD (and/or electron diffraction) measurements of the aligned sample are needed for a more conclusive study in the future. The peak at 0.406 nm can be correlated to the distance between the aliphatic chains by van der Waals interactions. In the small-angle region, the reflection peaks can be roughly correlated to a 2D monoclinic unit cell with parameters $a = 2.345$ nm, $b = 1.90$ nm, and $\gamma = 84^\circ$. Because of complicated three-dimensional (3D) intermolecular correlations and the lack of single-crystal

(44) (a) Andersen, T. L.; Krebs, F. C.; Thorup, N.; Bechgaard, K. *Chem. Mater.* **2000**, *12*, 2428. (b) Fischbach, I.; Pakula, T.; Minkin, P.; Fechtenkötter, A.; Müllen, K.; Spiess, H. W.; Saalwacher, K. *J. Phys. Chem. B* **2002**, *106*, 6408. (c) Minch, B. A.; Xia, W.; Donley, C. L.; Hernandez, R. M.; Carter, C.; Carducci, M. D.; Dawson, A.; O'Brien, D. F.; Armstrong, N. R. *Chem. Mater.* **2005**, *17*, 1618. (d) Elmahdy, M. M.; Dou, X.; Mondeshki, M.; Floudas, G.; Butt, H.-J.; Spiess, H. W.; Müllen, K. *J. Am. Chem. Soc.* **2008**, *130*, 5311.

structure, only a few reflections were assigned and the experimental data agreed well with the calculated data (see Table 2). The XRD pattern measured at 70 °C after slow cooling from 125 °C show less reflection peaks, and the peaks correlated to the π -stacking disappeared (see Figure 7B), indicating that only short-range columnar

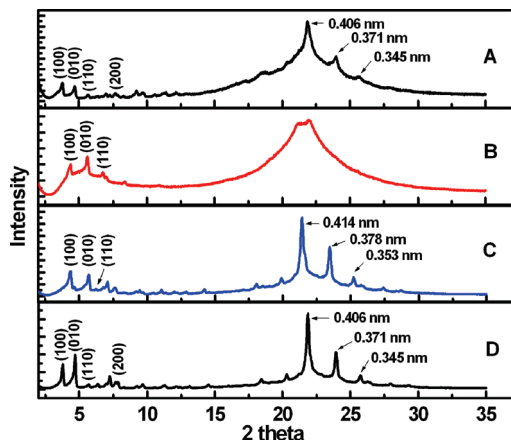


Figure 7. Variable-temperature X-ray diffraction (VT-XRD) patterns for TP-TATC6: at room temperature (pristine film) (spectrum A), at 70 °C (spectrum B), at 50 °C (spectrum C), and at room temperature after slow cooling from 125 °C (spectrum D). The samples are annealed for 300 s at the respective temperatures before X-ray measurement.

stacking is observed in this columnar liquid crystalline phase. The reflection peaks in the small-angle region can be correlated to a 2D monoclinic unit cell with parameters $a = 2.03$ nm, $b = 1.55$ nm, and $\gamma = 84^\circ$ (see Table 2). These reflection peaks were not observed in the XRD pattern measured at above 101 °C, due to the weak intermolecular associations in a less-ordered nematic DLC phase. The XRD pattern at 50 °C upon further cooling showed many reflection peaks (see Figure 7C), indicating a crystalline phase. The π -stacking distance (0.353 nm) is slightly larger than that at room temperature, and a 2D monoclinic unit cell can be determined with parameters $a = 2.02$ nm, $b = 1.57$ nm, and $\gamma = 84^\circ$ (see Table 2). Further slow cooling to room temperature resulted in more sharper reflection peaks, compared with those of the pristine sample (see Figure 7D), suggesting that thermal annealing improved the molecular order. Besides these changes, their unit-cell parameters and π -stacking distance are almost the same (see Table 2).

The POM measurement showed that the TP-TATC12 entered into an isotropic phase (I) above 115 °C. After slow cooling from the isotropic phase, a typical fan-type texture was observed at 95 °C (Figure 8A), indicating a possible hexagonal columnar liquid crystalline phase (Col_h). Upon further cooling to 68 °C, the liquid crystals

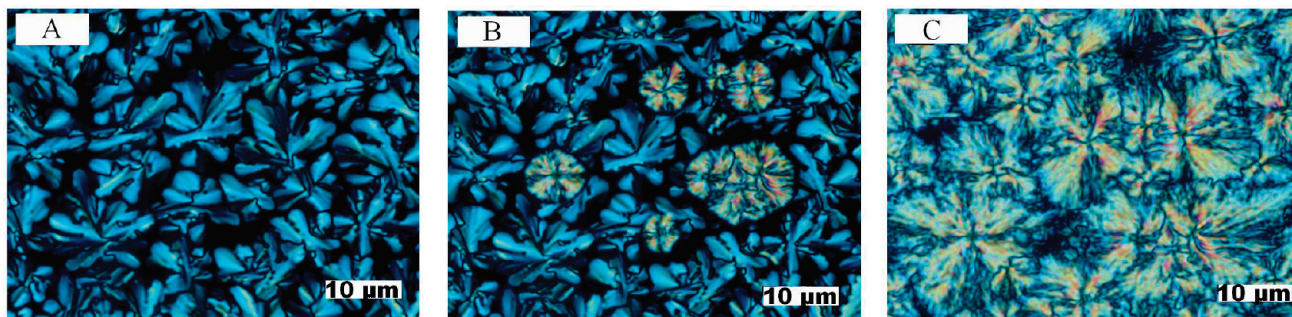


Figure 8. POM images of the drop-casted thin film of TP-TATC12 between two glass slides observed under two crossed polarizers upon slow cooling from the isotropic phase: (A) at 95 °C, (B) at 68 °C, and (C) at 63 °C.

Table 2. Variable-Temperature X-ray Diffraction (VT XRD) Data for TP-TATC6 and TP-TATC12

temperature (°C)	mesophase	cell	Lattice Parameters					d Spacing [nm]		Miller indices
			a [nm]	b [nm]	α (deg)	β (deg)	γ (deg)	observed	calculated	
TP-TATC6										
70	Col	monoclinic	2.03	1.55	90	90	84	2.02	2.02	100
								1.55	1.54	010
								1.30	1.29	110
50	K	monoclinic	2.03	1.57	90	90	84	2.02	2.02	100
								1.57	1.56	010
								1.31	1.30	110
25	K	monoclinic	2.345	1.90	90	90	84	2.34	2.33	100
								1.88	1.89	010
								1.54	1.55	110
								1.15	1.17	200
TP-TATC12										
85	Col_h	hexagonal	5.96	5.96	90	90	120	2.95	2.98	110
								2.60	2.58	200
25	K	monoclinic	3.97	3.4	90	90	82	2.55	2.54	100
								2.97	2.97	010
								3.63	3.63	110
								5.52	5.52	210
								5.94	5.94	020

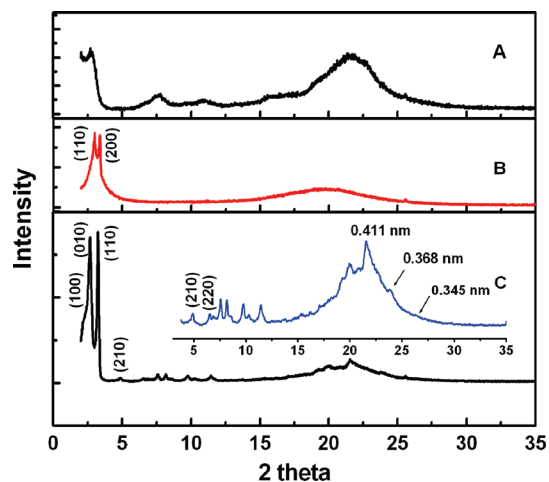


Figure 9. VT-XRD patterns for TP-TATC12: as-prepared sample (spectrum A), at 85 °C after slow cooling from 120 °C (spectrum B), and at room temperature after slow cooling from 120 °C (spectrum C). The samples were annealed for 300 s at the respective temperatures before X-ray measurement.

start to crystallize into spherical crystals (Figure 8B) and all the materials form crystals when the temperature is reduced to 63 °C (Figure 8C). Such clear phase transitions from a crystalline phase (K) to a hexagonal columnar liquid crystalline phase (Col_h) and then to an isotropic phase are consistent with the DSC data. Similarly, the VT XRD measurements were conducted and the diffraction patterns are shown in Figure 9. The XRD pattern of the pristine sample at room temperature show broad reflections, likely because of the existence of polymorphism in the as-prepared sample (see Figure 9A). To obtain better-resolved patterns, thermal annealing was done. When the sample was measured at 85 °C after slow cooling from the isotropic phase, two intense reflection peaks in the small-angle region were observed and only a halo was observed in the wide-angle region (see Figure 9B). The peaks in the small-angle region can be correlated to the distances of the (110) and (200) reflection planes of a 2D hexagonal unit cell with parameters $a = b = 5.96$ nm and $\gamma = 120^\circ$ (see Table 2). However, the (100) reflection peak is outside of the determination limit. These data also agree well with the fan-type texture observed in the POM measurements. Upon further cooling to room temperature, many sharp reflection peaks were observed (see Figure 9C), indicating that thermal annealing helps these disklike molecules to self-organize into a more-ordered superstructure. Reflection peaks correlated to the perpendicular π -stacking distance (0.345 nm) was also observed. The reflection peaks in the small-angle region can be assigned to a 2D monoclinic unit cell with parameters $a = 3.97$ nm, $b = 3.4$ nm, and $\gamma = 82^\circ$ (see Table 2).

Based on the aforementioned data, we can conclude that both TP-TATC6 and TP-TATC12 have very good thermal stability and they exhibit typical thermotropic liquid crystalline behavior with different mesophases. Annealing of the bulk materials in the liquid crystalline phase can improve their molecular order and highly ordered columnar superstructures at room temperature

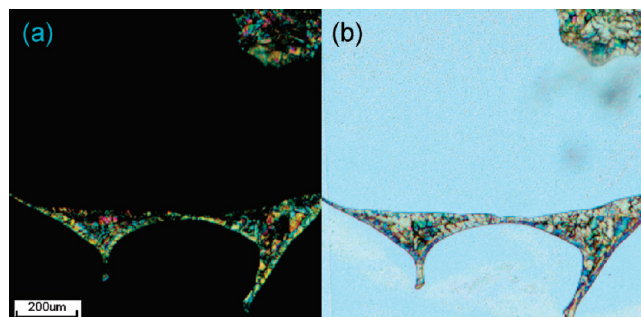


Figure 10. Micrographs of TP-TATC12 sandwiched between two ITO electrodes after slow cooling to room temperature from isotropic phase: (a) under cross polarizers and (b) without polarizer.

can be achieved. All these are important for their practical applications in electronic devices.

Space-Charge Limited-Current (SCLC) Mobility Measurements. The charge carrier mobilities of TP-TATC6 and TP-TATC12 were obtained using the space-charge limited-current (SCLC) technique. The SCLC measurements were made in a cross-junction ITO/material/ITO cell, with a thick film of the discotic semiconductor sandwiched between two lithographically patterned ITO glass electrodes. (Here, ITO is indium tin oxide.) The solid materials were loaded onto a hot bottom ITO electrode to facilitate materials transfer, before closing with the top ITO electrode. TP-TATC6 powder was loaded with the bottom ITO electrode at 140 °C, and TP-TATC12 was loaded at 120 °C. The thickness of the material was approximately defined by the thickness of the lithographically patterned SU8 spacer and the actual thickness was obtained from the interference fringe spacing of the air gap adjacent to the materials. The TP-TATC6 device was then annealed to 140 °C, cooled at a rate of 0.1 °C/min to 70 °C, then cooled at a rate of 1 °C/min to room temperature. The TP-TATC12 device was annealed to 120 °C, similarly cooled at a rate of 0.1 °C/min to 90 °C, then at a rate of 5 °C/min to room temperature. The micrographs (both polarized and unpolarized) of the morphology of the materials disclosed that homeotropic domains (with columnar alignment perpendicular to the surfaces) were observed for both compounds (see Figure 10, with compound TP-TATC12 as an example). Such a homeotropic alignment of discotic molecules was promoted by slow cooling. In contrast, faster cooling (5 °C/min) led to thin films with the discs in an edge-on alignment, as observed by POM. The active area for the device was then obtained from the overlap between the homeotropic phase and the electrodes with a pixel-counting software.

The current–voltage characteristics were measured in a glovebox at room temperature (Keithley, Model 4200). In a typical experiment, the thicknesses of the TP-TATC6 and TP-TATC12 are 25 and 42 nm, respectively, and the device areas are 0.194 mm² and 0.025 mm², respectively. Current–voltage measurements (Figure 11) exhibit a typical linear region at low voltages, where the behavior is ohmic, and a quadratic region at higher voltages, where the current becomes space-charge-limited. Therefore, the SCLC mobility can be calculated from $J = \frac{9}{8} \frac{\epsilon_0 \epsilon_r \mu V^2}{d^3}$ –

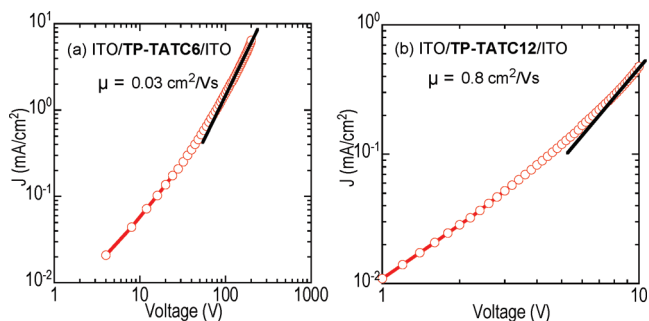


Figure 11. Double logarithmic plot of the current density (J) versus applied voltage (V) measured in (a) a 25- μm -thick sample of **TP-TATC6** and (b) a 42- μm -thick sample of **TP-TATC6**, each at room temperature, after slow cooling from the isotropic phase. Symbols represent experimental data and the continuous lines represent ideal quadratic regimes of the current, as a function of the applied voltage.

where J is the measured current density, μ the charge mobility, ϵ_0 the permittivity of free space, ϵ_r the dielectric constant of the material (a value of $\epsilon_r = 3$ is assumed here), V the applied voltage, and d the thickness of the device. The SCLC mobilities were obtained to be 0.03 and 0.8 $\text{cm}^2/(\text{V s})$ for **TP-TATC6** and **TP-TATC12**, respectively. These values are higher than those for most other DLCs, likely because of the ordered homeotropic alignment of the discs under our conditions. In particular, to the best of our knowledge, the **TP-TATC12** possesses the highest SCLC mobility among all DLCs, including the small-size TAT-based liquid crystals.^{35a}

Gelation Behavior of TP-TATC12. Compounds **TP-TATC6** and **TP-TATC12** are readily soluble in chloroform, DCM, and THF, but they are insoluble in some alcohol and ester solvents, such as ethanol and ethyl acetate. Meanwhile, they can be slowly dissolved in aliphatic hydrocarbon solvents such as cyclohexane, *n*-hexane, and *n*-decane, upon heating. During the solubility test of these compounds in different solvents, we found that **TP-TATC12** could form transparent and luminescent organic gel in certain solvents (see Figure 12), whereas the short-chain-substituted **TP-TATC6** did not show any gelation behavior. This is a very unusual phenomenon, because the formation of most organic gels is due to the existence of strong secondary interactions such as hydrogen bonding,⁴⁵ and there are only very few

exceptions where physical gels are formed due to π – π interactions or dipole–dipole interactions.⁴⁶ In the case of the **TP-TATC12**, intermolecular hydrogen bonding does not exist and the most significant secondary interaction is believed to be π – π interactions between the disklike core molecules. The gelation behavior of **TP-TATC12** was tested in different solvents (see Table 3) by heating the solutions in an oil bath to fully dissolve the sample and then allow the solutions to slowly cool to room temperature. It was found that transparent organic gels were formed in nonpolar hydrocarbon solvents, such as hexane and toluene, and some aliphatic alcohols and esters, such as 1-hexanol and *n*-butyl acetate, with critical gelation concentrations (usually < 3.5 mg/mL). However, only precipitates were formed in ethanol and acetone and homogeneous solutions were formed in DCM and THF. Gels can also be generated in mixed solvents such as hexane/DCM (4:1, v/v). It is known that, in nonpolar hydrocarbon solvents, the intermolecular π – π interactions are stronger than those in polar solvents such as DCM and THF, as previously observed in many aromatic discotic mesogens.^{3h,47} Such strong π – π interactions in solution will result in columnar structures above a critical concentration. The intercolumnar interactions (e.g., by van der Waals interactions) will lead to a 3D network, which then gels the organic solvents. Herein, the long aliphatic alkyl chains in **TP-TATC12** are supposed to enhance the intercolumnar association, especially in nonpolar hydrocarbon solvents. In contrast, the shorter aliphatic-chain-substituted **TP-TATC6** does not show any gelation behavior. In the polar aliphatic alcohols and esters, the nonpolar side of the solvent molecules is believed to interact with the aliphatic chains of the **TP-TATC12** in the self-assembled columns via van der Waals interactions, while the polar head ($-\text{OH}$ or $-\text{OAc}$) points outside to provide additional intercolumnar hydrogen bonding (for alcohol) or dipole–dipole (for ester) interactions. The critical gelation concentration in toluene (3.5 mg/mL) is larger than that in other aliphatic hydrocarbon, alcohol, and ester solvents (< 2.5 mg/mL), probably because of the negative interactions between the aromatic toluene solvents and the aromatic discotic mesogens.

To further understand the gelation behavior, the morphology of the xerogel and the film of **TP-TATC12** prepared by drop-casting its toluene solution onto a copper substrate was investigated by scanning electron microscopy (SEM). In the xerogel, a 3D network of shranked layerlike microstructures was observed (see Figure 12A). In the drop-casted thin films, fibrous microstructures several micrometers in width and tens of micrometers in length were observed, which formed a 3D cross-linking network (see Figure 12B). Both microstructures are desirable to gelate organic solvents among the network, and, thus, physical gels are formed. For

- (45) (a) Terech, P. R.; Weiss, G. *Chem. Rev.* **1997**, *97*, 3133. (b) Brunsveld, L.; Folmer, B. J. B.; Meijer, E. W.; Sijbesma, R. P. *Chem. Rev.* **2001**, *101*, 4071. (c) Camerel, F.; Bonardi, L.; Schmutz, M.; Ziessel, R. *J. Am. Chem. Soc.* **2006**, *128*, 4548. (d) Chen, Z.; Baumeister, U.; Tschierske, C.; Würthner, F. *Chem.—Eur. J.* **2007**, *13*, 450. (e) Sagara, Y.; Kato, T. *Angew. Chem., Int. Ed.* **2008**, *47*, 5175. (f) de Greef, T. F. A.; Meijer, E. W. *Nature* **2008**, *453*, 171. (g) Yasuda, T.; Ooi, H.; Morita, J.; Akama, Y.; Minoura, K.; Funahashi, M.; Shimomura, T.; Kato, T. *Adv. Funct. Mater.* **2009**, *19*, 411. (46) (a) Brotin, T.; Utermöhlen, R.; Fages, F.; Bouas-Laurent, H.; Desvergne, J.-P. *J. Chem. Soc., Chem. Commun.* **1991**, 416. (b) Clavier, G.; Mistry, M.; Fages, F.; Pozzo, J. L. *Tetrahedron Lett.* **1999**, *40*, 9021. (c) Würthner, F.; Yao, S.; Beginn, U. *Angew. Chem., Int. Ed.* **2003**, *42*, 3247. (d) Mamiya, J.; Kanie, K.; Hiyama, T.; Ikeda, T.; Kato, T. *Chem. Commun.* **2002**, 1870. (e) An, B.-K.; Lee, D.-S.; Lee, J.-S.; Park, Y.-S.; Song, H.-S.; Park, S. Y. *J. Am. Chem. Soc.* **2004**, *126*, 10232. (f) Zhi, L.-J.; Wu, J.-S.; Müllen, K. *Org. Lett.* **2005**, *7*, 5761. (g) Lee, D.-C.; McGrath, K. K.; Jang, K. *Chem. Commun.* **2008**, 3636. (h) Haino, T.; Tanaka, M.; Fukazawa, Y. *Chem. Commun.* **2008**, 468. (i) Varghese, S.; Nambalan, S.; Kumar, S.; Krishna, A.; Doddamane, S.; Rao, S.; Prasad, S. K.; Das, S. *Adv. Funct. Mater.* **2009**, *19*, 1.

- (47) (a) Wu, J.-S.; Fechtenkötter, A.; Gauss, J.; Watson, M. D.; Kastler, M.; Fechtenkötter, C.; Wagner, M.; Müllen, K. *J. Am. Chem. Soc.* **2004**, *126*, 11311. (b) Pisula, W.; Tomović, Z.; Simpson, C. D.; Kastler, M.; Pakula, T.; Müllen, K. *Chem. Mater.* **2005**, *17*, 4296.

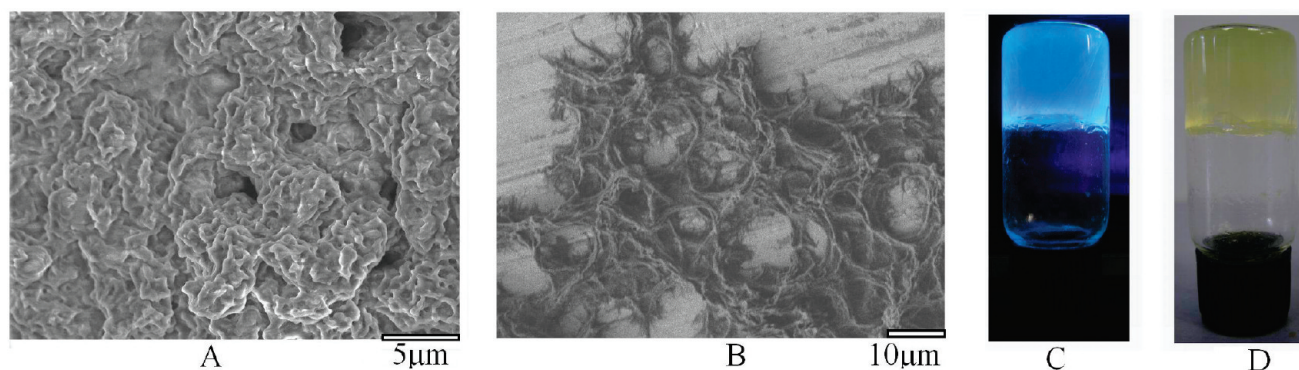


Figure 12. SEM images of (A) TP-TATC12 in the xerogel and (B) TP-TATC12 thin films prepared by drop-casting a toluene solution onto a copper substrate. Also shown are photographs of the organic gel formed in toluene under (C) a UV lamp (excited with 365-nm light) and (D) natural light.

Table 3. Gelation Testing Results of TP-TATC12 in Different Organic Solvents

solvent	status ^a
hexane	G
toluene	G
hexanol	G
butyl acetate	G
hexane/DCM (4/1, v/v)	G
ethanol	I
acetone	I
DCM	S
THF	S

^aLegend: G = gel, S = soluble, and I = insoluble.

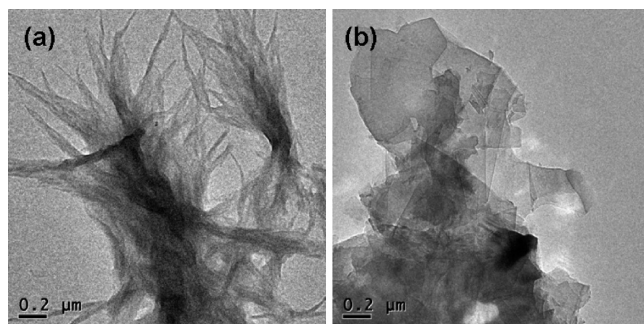


Figure 13. TEM images of the TP-TATC12 under different conditions: (a) a solution of TP-TATC12 in hexane (1×10^{-4} M) was aged for 3 days and dropped onto a copper TEM grid; (b) a solution of TP-TATC12 in toluene (1×10^{-4} M) was aged for 3 days and dropped onto a copper TEM grid.

comparison, the TPC6 and TATC12 do not show any gelation behavior. This unusual gel formation from TP-TATC12 further indicates that there are strong intermolecular interactions in the newly designed TP-fused TAT mesogens.

Such a unique gelation process observed for TP-TATC12 must be related to the preorganization of the molecules in solution. Thus, the solutions of TP-TATC12 in hexane and toluene (both with a concentration of 10^{-4} M) were aged at room temperature for 3 days and the aged solutions were deposited dropwise onto a 300 mesh copper grid for transmission electron microscopy (TEM) measurement. Interestingly, the sample prepared from the aged hexane solution showed many fibrous nanostructures, while the sample prepared from toluene

displayed thin sheets hundreds of nanometers in thickness (see Figure 13). Although it is not easy to understand such a structural difference at this moment, the strong association between the nanofibers or the nanosheets is believed to play important roles in the gelation of the organic solvents. In contrast, the TEM measurements of the samples of TP-TATC6 under the same preparation conditions only disclosed some irregular particles. As a result, TP-TATC6 cannot form gels in the tested solvents.

Conclusions

In summary, we have developed a new family of enlarged π -conjugated discotic mesogens via the fusion of three triphenylene (TP) units onto a triazatruxene (TAT) core. The newly formed large discotic molecules TP-TATC6 and TP-TATC12 combine the electronic and self-assembling properties of both TP and TAT. Extended π -conjugation with desirable HOMO energy levels suitable for charge injection from electrodes was observed for the new materials. These disklike molecules have very good thermal stability and exhibit thermotropic liquid crystalline behavior. Highly ordered columnar superstructures were observed when cooled from liquid crystalline phases. High space-charge limited-current (SCLC) charge carrier mobilities were obtained for TP-TATC6 and TP-TATC12. In addition, an unusual gelation behavior of TP-TATC12 in different solvents was observed, further proving the strong intermolecular interactions in the new π -systems. The facile synthesis, the intriguing electronic property, the ordered self-assembly, and the high SCLC mobilities of this new type of material qualify them as potential electrode-friendly hole-transporting semiconductors for electronic devices, such as field-effect transistors, light-emitting diodes, and solar cells. Research on their self-assembly at the solid/liquid interface and their device application is ongoing in our group.

Experimental Section

Materials and Methods. All chemicals, reagents, and solvents from commercial sources were used as received without further purification, except anhydrous THF, which was distilled over

sodium prior to use. The hexabromo-triazatruxene (**1**) was synthesized as described previously.³⁰ **2a** was prepared in 82% yield, according to the reported procedure.^{34d} Column chromatography was performed on silica gel 60 (Merck 40–60 nm, 230–400 mesh). Microwave-assisted reactions were performed using a CEM Discovery single-mode focused-microwave system. The pressure was controlled by a load cell connected to the vessel via a septum. The temperature of the contents in the vessel was monitored using a calibrated IR temperature controller mounted under the reaction vessel.

All NMR spectra were recorded on Bruker spectrometers (Model AMX500 at 500 MHz and a Model ACF300 at 300 MHz). All chemical shifts are quoted in parts per million (ppm), relative to tetramethylsilane, using the residual solvent peak as a reference standard. EI-MS were recorded on Finnigan TSQ 7000 triple-stage quadrupole mass spectrometer. MALDI-TOF mass spectra were measured on a Bruker Autoflex MALDI-TOF instrument, using 1,8,9-trihydroxyanthracene as a matrix. Elemental analysis (C, H, N) was performed on a Vario EL Elemental system (Elementar Analyzen-systeme, Hanau, Germany). UV-vis absorption and fluorescence spectra were recorded on a Shimadzu Model UV-1700 spectrometer and a Shimadzu Model RF-5301 fluorometer, respectively. Cyclic voltammetry (CV) was performed on a CHI Model 620C electrochemical analyzer with a standard three-electrode cell in dry DCM with 0.1 M tetrabutylammonium hexafluorophosphate (TBAPF₆) as the supporting electrolyte, and the scan rate was 50 mV/s. A gold disk electrode 2 mm in diameter, a platinum wire, and a AgCl/Ag electrode were used as the working electrode, the counter electrode, and the reference electrode, respectively.

Thermogravimetric analysis (TGA) was conducted on a TA Instruments Model 2960 system at a heating rate of 10 °C/min under a nitrogen flow. Differential scanning calorimetry (DSC) was performed on a TA Instruments Model 2920 apparatus at a heating/cooling rate of 10 °C/min under a nitrogen flow. Polarizing optical microscopy (POM) images of the samples sandwiched between two glass slides were recorded on the Olympus Model BX51 equipped with the Linkam TP94 programmable hot stage. Variable-temperature X-ray diffraction (VT XRD) studies were performed on a Bruker-AXS D8 ADVANCE powder X-ray diffractometer with an Anton Paar Model HTK 1200 high-temperature chamber, and the room-temperature XRD measurements were performed on a Bruker-AXS D8 DISCOVER system with a GADDS powder X-ray diffractometer, both with Cu K α radiation. Transmission electron microscopy (TEM) measurements were conducted on a JEOL Model 2010 FEG microscope at 200 keV.

Synthesis of 1,2-bis(hexyloxy)benzene (5a). In a three-neck flask, a mixture of pyrocatechol (6.40 g, 58.1 mmol), K₂CO₃ (40.1 g, 290 mmol), KI (0.1 g, 0.6 mmol), and 1-bromohexane (20.01 g, 122.01 mmol) in acetone (150 mL) was heated to 65 °C for 48 h with stirring under a nitrogen atmosphere. After cooling to room temperature, the solvent was removed under vacuum and 10% NaOH (200 mL) was added. The mixture was extracted with DCM (2 \times 150 mL), and the combined organic layer was washed by water, brine, and dried over MgSO₄. The solvent was removed under vacuum and the residue was purified by column chromatography (silica gel, hexane/DCM = 6:1, v/v) to give the title product as a colorless oil in 90% yield. ¹H NMR (300 MHz, CDCl₃, δ ppm): 6.89 (br, 4H, Ar-H), 4.00 (t, *J* = 6.6 Hz, 4H, OCH₂-), 1.87–1.77 (m, 4H), 1.53–1.44 (m, 4H), 1.38–1.32 (br, 8H), 0.91 (t, *J* = 6.9 Hz, 6H, -CH₃). ¹³C NMR (75 MHz, CDCl₃, δ ppm): 149.21, 120.93, 114.05, 69.18, 31.57,

29.27, 25.67, 22.56, 13.95. HR-EI MS (*m/z*): found, 278.2273 (M⁺); calcd for C₁₈H₃₀O₂, 278.2246.

Synthesis of 1,2-bis(dodecyloxy)benzene (5b). Compound **5b** was synthesized according to a similar procedure to **5a**. The crude product precipitated upon cooling in acetone, and it was recrystallized in ethanol to give the title product **5b** in 88% yield. ¹H NMR (300 MHz, CDCl₃, δ ppm): 6.88 (br, 4H, Ar-H), 3.99 (t, *J* = 6.6 Hz, 4H, OCH₂-), 1.85–1.78 (m, 4H), 1.46–1.26 (br, 36H), 0.88 (t, *J* = 6.0 Hz, 6H, -CH₃); ¹³C NMR (75 MHz, CDCl₃, δ ppm): 149.32, 121.02, 114.27, 69.35, 31.92, 29.69, 29.63, 29.45, 29.37, 26.06, 22.68, 14.07. HR-EI MS (*m/z*): found, 446.4572 (M⁺); calcd for C₃₀H₅₄O₂, 446.4424.

Synthesis of 4-bromo-1,2-bis(hexyloxy)benzene (6a). *N*-bromosuccinimide (2.02 g, 11.3 mmol) was added to a solution of **5a** (3.0 g, 10.8 mmol) in THF (50 mL). The mixture was stirred under darkness at room temperature overnight. The pale yellow mixture was poured into water (200 mL) and extracted by ethyl acetate (3 \times 50 mL). The organic layer was washed by brine and dried over anhydrous Na₂SO₄. The solvent was removed under vacuum and the obtained yellow oil was purified by column chromatography (silica gel, hexane/DCM = 6:1, v/v) to give pure **6a** as a colorless oil in 95% yield. ¹H NMR (300 MHz, CDCl₃, δ ppm): 7.00–6.96 (m, 2H), 6.75–6.72 (m, 1H), 3.98–3.93 (m, 4H), 1.85–1.74 (m, 4H), 1.48–1.33 (br, 12H), 0.92–0.88 (m, 6H). ¹³C NMR (75 MHz, CDCl₃, δ ppm): 150.09, 148.42, 123.45, 117.03, 115.25, 112.80, 69.57, 69.41, 31.56, 31.53, 29.19, 29.11, 25.65, 22.58, 13.98. HR-EI MS (*m/z*): found, 357.1382 ([M+H⁺]); calcd for C₁₈H₂₉BrO₂, 356.1351.

Synthesis of 4-bromo-1,2-bis(dodecyloxy)benzene (6b). Compound **6b** was prepared according to a similar procedure to **6a**. The crude product was purified by crystallization in ethanol to give pure **6b** as a needlelike solid in 95% yield. ¹H NMR (300 MHz, CDCl₃, δ ppm): 7.00–6.96 (m, 2H), 6.75–6.72 (m, 1H), 3.98–3.93 (m, 4H), 1.85–1.74 (m, 4H), 1.45–1.26 (br, 32H), 0.90–0.86 (m, 6H). ¹³C NMR (75 MHz, CDCl₃, δ ppm): 150.07, 148.39, 123.42, 117.01, 115.21, 112.80, 69.51, 69.36, 31.91, 29.68, 29.64, 29.60, 29.39, 29.35, 29.23, 29.15, 25.98, 22.67, 14.07. HR-EI MS (*m/z*): found, 524.3309 ([M+H⁺]); calcd for C₃₀H₅₃BrO₂, 524.3229.

Synthesis of 2-(3,4-bis(hexyloxy)phenyl)-4,4,5,5-tetramethyl-1,3,2-dioxaborolane (3a). A solution of **5a** (10.0 g, 28.07 mmol) in dry THF (150 mL) was cooled to -78 °C in a dry ice/acetone bath. Then, *n*-butyl lithium (19.30 mL, 1.6 M in hexane, 30.8 mmol) was added dropwise via a syringe and the solution was allowed to warm to room temperature for 1 h. The solution was recooled to -78 °C before 2-isopropoxy-4,4,5,5-tetramethyl-1,3,2-dioxaborolane (5.86 g, 31.5 mmol) was added via a syringe at one portion. The mixture was then allowed to slowly warm to room temperature and stirred for 24 h. The mixture was extracted with diethyl ether (2 \times 100 mL), and the combined organic layer was washed with brine and dried over Na₂SO₄. The solvent was removed under vacuum and the obtained pale yellow oil was purified by column chromatography (silica gel, hexane/DCM = 3:1, v/v) to give pure **3a** as a colorless oil in 85% yield. ¹H NMR (300 MHz, CDCl₃, δ ppm): 7.38 (dd, ³*J* = 7.8, ⁴*J* = 1.5 Hz, 1H), 7.29 (d, *J* = 1.5, 1H), 6.87 (d, *J* = 7.8 Hz, 1H), 4.05–3.99 (m, 4H, OCH₂-), 1.86–1.76 (br, 4H, OCH₂-CH₂-), 1.49–1.24 (br, 24H), 0.92–0.88 (br, 6H, -CH₃). ¹³C NMR (75 MHz, CDCl₃, δ ppm): 152.00, 148.55, 128.63, 119.55, 112.78, 83.54, 69.27, 68.90, 31.61, 31.57, 29.36, 29.17, 25.72, 25.67, 24.84, 24.80, 22.60, 14.00. HR-EI MS (*m/z*): found, 405.3107 ([M+H⁺]); calcd for C₂₄H₄₁BO₄, 404.3098.

Synthesis of 2-(3,4-bis(dodecyloxy)phenyl)-4,4,5,5-tetramethyl-1,3,2-dioxaborolane (3b). Compound **3b** was prepared according

to a similar procedure to **3a**. It was purified by column chromatography (silica gel, hexane/DCM = 3:1, v/v) to give pure **3b** as a white solid in 69% yield. ¹H NMR (300 MHz, CDCl₃, δ ppm): 7.37 (d, *J* = 8.1 Hz, 1H, Ar-H), 7.29 (s, 1H, Ar-H), 6.87 (d, *J* = 8.1 Hz, 1H, Ar-H), 4.05–3.99 (m, 4H, OCH₂-), 1.86–1.77 (m, 4H, OCH₂-CH₂-), 1.46–1.26 (br, 48H), 0.90–0.86 (br, 6H, -CH₃). ¹³C NMR (75 MHz, CDCl₃, δ ppm): 151.98, 148.54, 128.63, 119.54, 112.77, 83.51, 69.26, 68.88, 31.91, 29.68, 29.63, 29.60, 29.43, 29.41, 29.35, 29.20, 26.05, 25.99, 24.83, 22.67, 14.07. HR-EI MS (*m/z*): found, 573.4803 ([*M*+H⁺]); calcd for C₃₆H₆₅BO₄, 572.4976.

Synthesis of 2,3,7,8,12,13-hexabromo-5,10,15-tridodecyl-10,15-dihydro-5H-diindolo[3,2-a:3',2'-c]carbazole (2b). A mixture of **1** (2.47 g, 3.02 mmol) and KOH (2.52 g, 45 mmol) in THF (50 mL) was heated to 70 °C and the 1-bromododecane (2.48 g, 10.0 mmol) was added. The solution was kept refluxing for 12 h under a nitrogen atmosphere, before it was cooled to room temperature. The mixture was diluted with DCM (150 mL) and washed with 10% HCl (2 × 100 mL) and then brine. The organic layer was dried over Na₂SO₄, and the solvents were removed under vacuum. The residue was purified by column chromatography (silica gel, hexane/DCM = 8:1, v/v) to give pure **2a** as a pale white solid (2.94 g, 74%). ¹H NMR (300 MHz, CDCl₃, δ ppm): 8.21 (s, 3H), 7.69 (s, 3H), 4.37 (t, *J* = 4.8 Hz, 6H), 1.86 (br, 6H), 1.29–1.20 (br, 54H), 0.88 (t, *J* = 4.5 Hz, 9H). ¹³C NMR (75 MHz, CDCl₃, δ ppm): 139.81, 138.40, 124.71, 122.52, 118.47, 115.17, 114.24, 100.97, 46.71, 31.94, 30.22, 29.68, 29.65, 29.61, 29.57, 29.52, 29.38, 29.30, 26.43, 22.71, 14.13. MALDI-TOF MS (*m/z*): found, 1318.64 ([*M*+H⁺]), 1239.47 ([*M*-Br+H⁺]), 1159.28 ([*M*-2Br + H⁺]), 1079.96 ([*M*-3Br+H⁺]), 1001.25 ([*M*-4Br+H⁺]), 923.21 ([*M*-5Br+H⁺]), 844.96 ([*M*-6Br+H⁺]); calcd for C₆₀H₈₁Br₆N₃ (exact mass), 1317.15.

Synthesis of 2,3,7,8,12,13-hexakis(3,4-bis(hexyloxy)phenyl)-5,10,15-trihexyl-10,15-dihydro-5H-diindolo[3,2-a:3',2'-c]carbazole (4a). A mixture of **3a** (0.53 g, 0.5 mmol), **2a** (1.58 g, 3.9 mmol), and Cs₂CO₃ (1.95 g, 6.0 mmol) in toluene (10 mL) in a 10-mL pressure vessel was carefully degassed by purging through nitrogen before and after adding Pd(PPh₃)₄ (60 mg, 0.05 mmol). The vessel was then sealed and heated in the CEM Discover system. The initial microwave power was set at 100 W, and the reaction time was set as 30 min. The temperature was monitored using a calibrated infrared temperature controller mounted under the reaction vessel. The pressure was controlled by a load cell connected to the vessel via the septum. After the set temperature of 135 °C was reached, the microwave power regulated itself to keep that temperature before cooling to room temperature. The mixture was subsequently diluted with DCM (50 mL) and then washed with 1 M aqueous HCl (30 mL) and brine. The organic layer was dried over Na₂SO₄ and the solvent was removed under vacuum. The residue was purified by column chromatography (silica gel, hexane/DCM = 5/2, v/v) to give the pure **4a** in 82% yield. ¹H NMR (300 MHz, CDCl₃, δ ppm): 8.31 (s, 3H), 7.61 (s, 3H), 6.93 (d, *J* = 8.1 Hz, 6H), 6.86 (d, *J* = 8.1 Hz, 6H), 6.76–6.71 (m, 6H), 4.95 (br, 6H), 4.02–3.97 (m, 12H), 3.75–3.70 (m, 12H), 2.09 (br, 6H), 1.79–1.87 (m, 12H), 1.71–1.65 (m, 12H), 1.49–1.08 (br, 84H), 0.95–0.88 (m, 42H), 0.74 (t, *J* = 6.9 Hz, 9H). ¹³C NMR (75 MHz, CDCl₃, δ ppm): 148.42, 147.82, 147.61, 140.44, 139.51, 136.00, 135.74, 135.48, 132.96, 123.21, 122.47, 122.19, 116.79, 116.656, 113.43, 111.48, 103.09, 69.34, 69.17, 69.07, 47.27, 31.66, 31.64, 31.57, 30.30, 29.41, 29.38, 29.14, 26.48, 25.76, 25.70, 22.632, 22.49, 13.99, 13.91. MALDI-TOF MS (*m/z*): found, 2254.92 ([*M*+H⁺]); calcd for C₁₅₀H₂₁₉N₃O₁₂ (exact mass), 2254.66. Elemental

analysis: calcd for C₁₅₀H₂₁₉N₃O₁₂: C 79.85, H 9.78, N 1.86, O 8.51; found: C 79.83, H 9.77, N 1.91.

Synthesis of 2,3,7,8,12,13-hexakis(3,4-bis(dodecyloxy)phenyl)-5,10,15-trihexyl-10,15-dihydro-5H-diindolo[3,2-a:3',2'-c]carbazole (4b). Compound **4b** was synthesized according to a similar procedure to **4a**. The crude product was purified by column chromatography (silica gel, hexane/DCM = 3/1, v/v) to give the pure **4b** in 74% yield. ¹H NMR (500 MHz, CDCl₃, δ ppm): 8.32 (s, 3H), 7.63 (s, 3H), 6.94 (d, *J* = 7.5 Hz, 6H), 6.86 (d, *J* = 7.5 Hz, 6H), 6.76–6.72 (m, 6H), 4.96 (br, 6H), 4.03–3.99 (m, 12H), 3.75–3.71 (m, 12H), 2.09 (br, 6H), 1.88–1.82 (m, 12H), 1.71–1.67 (m, 12H), 1.68–1.48 (m, 12H), 1.39–1.22 (br, 252H), 0.92–0.88 (m, 51H). ¹³C NMR (75 MHz, CDCl₃, δ ppm): 148.44, 147.85, 147.64, 140.44, 139.53, 136.03, 135.74, 135.53, 132.97, 124.45, 123.96, 123.23, 122.50, 122.19, 116.86, 116.75, 113.49, 111.49, 103.12, 69.41, 69.21, 69.12, 47.27, 31.94, 31.45, 30.32, 30.20, 29.75, 29.69, 29.54, 29.51, 29.39, 29.23, 26.78, 26.16, 26.11, 22.69, 14.08. MALDI-TOF MS (*m/z*): found, 3518.62 ([*M*+H⁺]); calcd for C₂₄₀H₃₉₉N₃O₁₂ (exact mass), 3516.07. Elemental analysis: calcd for C₂₄₀H₃₉₉N₃O₁₂: C 81.92, H 11.43, N 1.19, O 5.46; found: C 81.80, H 11.47 N 1.23.

Synthesis of TP-TATC6. A solution of **4a** (225 mg, 0.1 mmol) in dry DCM (80 mL) was degassed by bubbling through nitrogen gas for 15 min. FeCl₃ (228 mg, 1.4 mmol) in anhydrous CH₃NO₂ (0.5 mL) was then added dropwise via a syringe over the course of 15 min. The dark-green solution was kept stirring and bubbling with a nitrogen flow for 30 min and then the reaction was quenched with methanol (60 mL). The precipitate was collected and washed with methanol before dissolved in DCM (50 mL). The solution was washed with brine for twice and dried over Na₂SO₄. The solvent was removed under vacuum and the residue was purified by column chromatography (silica gel, hexane/DCM = 2/1, v/v) to give the title product **TP-TATC6** as a yellow powder (156 mg, 69%): ¹H NMR (500 MHz, CDCl₃, δ ppm): 9.43 (s, 3H), 8.67 (s, 3H), 8.35 (s, 3H), 8.27 (s, 3H), 7.96 (s, 3H), 7.95 (s, 3H), 5.38 (t, *J* = 7.0 Hz, 6H), 4.38 (m, 12H), 4.30 (m, 12H), 2.08–1.97 (m, 30H), 1.71–1.61 (m, 30H), 1.48–1.42 (m, 48H), 1.23–1.11 (m, 12H), 1.04–0.94 (m, 36H), 0.60 (t, *J* = 7.5 Hz, 9H). ¹³C NMR (125 MHz, CDCl₃, δ ppm): 149.62, 149.26, 149.21, 149.11, 141.73, 141.47, 125.92, 125.10, 124.38, 124.10, 123.78, 123.24, 115.68, 108.83, 108.58, 107.97, 107.74, 103.97, 103.25, 70.38, 70.12, 69.84, 69.78, 47.29, 31.77, 31.73, 31.27, 29.65, 29.53, 29.51, 29.11, 26.47, 25.99, 25.94, 25.92, 22.68, 22.31, 14.06, 13.72. MALDI-TOF MS (*m/z*): found, 2249.86 ([*M*+H⁺]); calcd for C₁₅₀H₂₁₃N₃O₁₂ (exact mass), 2248.61. Elemental analysis: calcd for C₁₅₀H₂₁₃N₃O₁₂: C 80.06, H 9.54, N 1.87, O 8.53; found: C 80.10, H 9.52, N 1.90.

Synthesis of TP-TATC12. Compound **TP-TATC12** was synthesized by a similar procedure to compound **TP-TATC6**. The crude product was purified by column chromatography (silica gel, hexane/DCM = 5:3, v/v) to give pure **TP-TATC12** as a yellow powder in 72% yield. ¹H NMR (500 MHz, CDCl₃, δ ppm): 9.44 (s, 3H), 8.67 (s, 3H), 8.35 (s, 3H), 8.27 (s, 3H), 7.95 (br, 6H), 5.39 (br, 6H), 4.42 (t, *J* = 6.3 Hz, 6H), 4.38 (t, *J* = 6.3 Hz, 6H), 4.31 (t, *J* = 6.3 Hz, 12H), 2.06–1.99 (m, 30H), 1.69–1.62 (m, 30H), 1.56–1.47 (m, 30H), 1.47–1.03 (br, 174H), 0.92–0.82 (br, 72H), 0.77 (t, *J* = 7.5, 9H). ¹³C NMR (125 MHz, CDCl₃, δ ppm): 149.57, 149.20, 149.15, 149.06, 141.73, 141.52, 125.93, 125.09, 124.38, 124.14, 123.76, 123.26, 115.69, 108.64, 108.46, 107.91, 107.69, 104.00, 103.29, 70.30, 70.09, 69.84, 69.77, 47.29, 31.95, 31.91, 31.81, 29.84, 29.79, 29.76, 29.74, 29.70, 29.61, 29.57, 29.51, 29.49, 29.42, 29.40, 29.38, 29.25, 29.17, 29.06, 26.77, 26.40, 26.36, 26.29, 22.70, 22.70, 22.66, 22.60, 14.12, 14.07, 14.04. MALDI-TOF MS (*m/z*): found, 3511.24

($[M+H]^+$), 3342.03 ($[M-C_{12}H_{25}+H]^+$); calcd for $C_{240}H_{393}N_3O_{12}$ (exact mass), 3510.02. Elemental analysis: calcd for $C_{240}H_{393}N_3O_{12}$: C 82.06; H 11.28, N 1.20, O 5.47; found: C 82.19, H 11.16, N 1.17.

Synthesis of 2,3,6,7,10,11-hexakis(hexyloxy)triphenylene (TPC6). A solution of **3a** (404 mg, 1.0 mmol) and 2 M CS_2CO_3 (3.75 mL, 7.5 mmol) in toluene (12 mL) in a 20-mL pressure vessel was carefully degassed by purging through nitrogen before and after adding $Pd(PPh_3)_4$ (68 mg, 0.06 mmol). After the set temperature of 150 °C was reached, the microwave power regulated itself to maintain that temperature for 40 min before cooling to room temperature. The mixture was subsequently diluted with DCM and then washed with 1 M aqueous HCl and saturated brine. The organic layer was dried over Na_2SO_4 and the solvent was removed under vacuum. The residue was purified by column chromatography (silica gel, hexane/ CH_2Cl_2 = 4/1, v/v) to give **TPC6** as a pale white solid in 75% yield. 1H NMR (300 MHz, $CDCl_3$, δ ppm): 7.84 (s, 6H), 4.23 (t, J = 6.6 Hz, 12H), 1.99–1.89 (m, 12H), 1.69–1.55 (m, 12H), 1.43–1.38 (m, 24H), 0.93 (t, J = 6.6 Hz, 18H). ^{13}C NMR (75 MHz, $CDCl_3$, δ ppm): 149.01, 123.64, 107.44, 69.74, 31.68, 29.44, 25.85, 22.65, 14.03. MALDI-TOF MS (m/z): found, 830.18 ($[M+H]^+$); calcd for $C_{54}H_{84}O_6$ (exact mass), 829.24. Elemental analysis: calcd for $C_{54}H_{84}O_6$: C 78.21, H 10.21, O 11.58; found: C 78.32, H 10.11.

Synthesis of 5,10,15-tridodecyl-10,15-dihydro-5H-diindolo-[3,2-a:3',2'-c]carbazole (TATC12). A mixture of **2b** (0.662 g, 0.5 mmol), Et_3N (0.55 mL, 4.0 mmol), $HCOOH$ (0.16 mL,

4.0 mmol), and 10% Pd/C (160 mg, 0.15 mmol) in THF (10 mL) was heated at 70 °C overnight. The mixture was filtered through Celite, and the filtrate was diluted with DCM. The solution was washed with aqueous HCl (10 mL), and the organic layer was dried over Na_2SO_4 . The solvent was removed under vacuum. The residue was purified column chromatography (silica gel, pure hexane) to give **TATC12** as a white solid (0.342 g, 80%). 1H NMR (500 MHz, $CDCl_3$, δ ppm): 8.30 (d, J = 8.0 Hz, 3H), 7.64 (d, J = 8.0 Hz, 3H), 7.45 (t, J = 8.0 Hz, 3H), 7.34 (t, J = 8.0 Hz, 3H), 4.92 (t, J = 8.0 Hz, 6H), 1.96 (quin, 6H), 1.19–1.29 (m, 54H), 0.89 (t, J = 8.0 Hz, 9H). ^{13}C NMR (125 MHz, $CDCl_3$, δ ppm): 141.04, 138.90, 123.51, 122.65, 121.49, 119.61, 110.50, 103.19, 47.03, 31.90, 29.77, 29.59, 29.58, 29.48, 29.44, 29.32, 29.23, 26.66, 22.68, 14.11. EI-MS (m/z): found, 849.9 (M^+); calcd for $C_{60}H_{87}N_3$, 849.69. Elemental analysis: calcd for $C_{60}H_{87}N_3$: C 84.75, H 10.31, N 4.94; found: C 84.85, H 10.20, N 4.82.

Acknowledgment. This work was financially supported by NRF Competitive Research Program (“Graphene-Related Materials and Devices”, No. R-143-000-360-281) and MOE AcRF Tier 1 FRC grant (No. R-143-000-370-112).

Supporting Information Available: NMR spectra of the various compounds discussed in this work, as well as MALDI-TOF mass spectra of the TP-modified TAT compounds. This material is available free of charge via the Internet at <http://pubs.acs.org>.